

# VOIGT–REUSS TOPOLOGY OPTIMIZATION FOR STRUCTURES WITH NONLINEAR MATERIAL BEHAVIORS

COLBY C. SWAN<sup>\*12</sup> AND IKU KOSAKA<sup>1</sup>

<sup>1</sup> *Department of Civil and Environmental Engineering, The University of Iowa, Iowa City, IA 52242, U.S.A.*

<sup>2</sup> *Center for Computer-Aided Design, The University of Iowa, Iowa City, IA 52242, U.S.A.*

## ABSTRACT

This work is directed toward optimizing concept designs of structures featuring inelastic material behaviours by using topology optimization. In the proposed framework, alternative structural designs are described with the aid of spatial distributions of volume fraction design variables throughout a prescribed design domain. Since two or more materials are permitted to simultaneously occupy local regions of the design domain, small-strain integration algorithms for general two-material mixtures of solids are developed for the Voigt (isostrain) and Reuss (isostress) assumptions, and hybrid combinations thereof. Structural topology optimization problems involving non-linear material behaviours are formulated and algorithms for incremental topology design sensitivity analysis (DSA) of energy type functionals are presented. The consistency between the structural topology design formulation and the developed sensitivity analysis algorithms is established on three small structural topology problems separately involving linear elastic materials, elastoplastic materials, and viscoelastic materials. The good performance of the proposed framework is demonstrated by solving two topology optimization problems to maximize the limit strength of elastoplastic structures. It is demonstrated through the second example that structures optimized for maximal strength can be significantly different than those optimized for minimal elastic compliance. © 1997 John Wiley & Sons, Ltd.

*Int. J. Numer. Meth. Engng.*, **40**, 3785–3814 (1997)

No. of Figures: 6. No. of Tables: 2. No. of References: 45.

KEY WORDS: topology optimization; structural optimization; design sensitivity analysis (DSA); nonlinear structures; mixtures

## 1. INTRODUCTION AND MOTIVATION

### 1.1. Overview

Variable topology material layout optimization is becoming an increasingly potent design tool in the layout of linear elastic structures for high stiffness,<sup>1–11</sup> in the design optimization of linear elastic composite materials,<sup>11–14</sup> and in the design of linear elastic structures for tailored eigenvalues.<sup>15–17</sup> In the so-called ‘structural topology optimization’ a fixed spatial design domain  $\Omega_D$  is designated as a subset of a full structural domain  $\Omega_S$ , and optimal spatial material distributions throughout  $\Omega_D$  are determined. Many variable topology material layout optimization frameworks today feature continuous formulations of the problem, in which either amorphous mixtures or microstructured mixtures (*composites*) are permitted to reside throughout  $\Omega_D$  in intermediate and even final design

\* Correspondence to: C. C. Swan, Department of Civil and Environmental Engineering, 2128 Engineering Building, The University of Iowa, Iowa City, IA 52242-1527, U.S.A.

states. Since it affects both the nature of the results obtained and the class of problems which can be feasibly attempted, an important facet of developing general methods to solve continuous variable topology material layout optimization problems is the choice of physical and constitutive treatment of the mixtures or composites. In Reference 18 a continuous structural topology optimization formulation was presented for linear elastic structures using amorphous mixtures of materials whose stress–strain behaviours are governed by classical Voigt and Reuss mixing rules. The objective of this paper is to extend the Voigt–Reuss topology formulation to the treatment of structures featuring materially non-linear inelastic behaviours.

### 1.2. Homogenization-based structural topology frameworks

Many very successful frameworks for continuous topology optimization of linear elastic structures treat biphasic mixtures of materials as composites characterized by parameterized micromorphologies.<sup>1, 2, 6–10</sup> To capture the effective response behaviour of such composites in structural analysis computations, effective medium constitutive models and their functional dependence upon microstructural design parameters are required. For general composites homogenized responses are often computed using classical micromechanics methods,<sup>19–21</sup> whereas for periodic composites effective medium responses are often computed with unit cell/homogenization frameworks.<sup>22–26</sup>

For the special case of linear, two-phased elastic composites (material phases  $\mathcal{A}$  and  $\mathcal{B}$  are both linear elastic and perfectly bonded), the functional form of the effective medium constitutive model will be that of linear, anisotropic elasticity, and standard methods can be employed to calculate the coefficients of the effective elasticity tensor  $\mathbf{C}^*$ . For example, in strain-controlled homogenization of linear elastic periodic composites<sup>22–26</sup> a macroscopic strain  $E_{kl}$  is imposed on the unit cell of the composite (Figure 1) and local equilibrium state equations  $\sigma_{ij,i} = 0$  are solved (subject to periodic boundary conditions) on the domain of the unit cell  $\bar{\Omega}_s$  for the microscale displacement field  $\mathbf{u}: \bar{\Omega}_s \mapsto \mathbb{R}^3$ . In solving the local equilibrium state equation over  $\bar{\Omega}_s$ , the local strain field  $\boldsymbol{\varepsilon}^{(kl)}(\mathbf{X})$  and the local stress field  $\boldsymbol{\sigma}^{(kl)}(\mathbf{X})$  are explicitly computed. By the average stress and strain theorems for composites subjected to macroscopically homogeneous strain  $E_{kl}$  loadings,<sup>27</sup> the corresponding macroscopic stress tensor  $S_{ij}^{(kl)}$  is simply the volume average of the local stress field

$$S_{ij}^{(kl)} = \frac{1}{V} \int_{\Omega_s} \sigma_{ij}^{(kl)} dV \quad (1)$$

Accordingly, by solving the unit cell problem for appropriate variations of the  $k$  and  $l$  indices of the macro strain tensor  $\mathbf{E}$ , the coefficients of the effective medium elastic stiffness tensor for the composite are simply

$$C_{ijkl}^* = \frac{S_{ij}^{(kl)}}{E_{kl}} \quad (2)$$

Due to the relative simplicity of such procedures, homogenization methods (the rigorous justification for which is presented in Reference 28) have gained strong acceptance in structural topology optimization of linear elastic structural systems.

In composites where one or more of the comprising materials feature inelastic behaviour, however, the homogenization procedures can become considerably more complicated. The difficulty

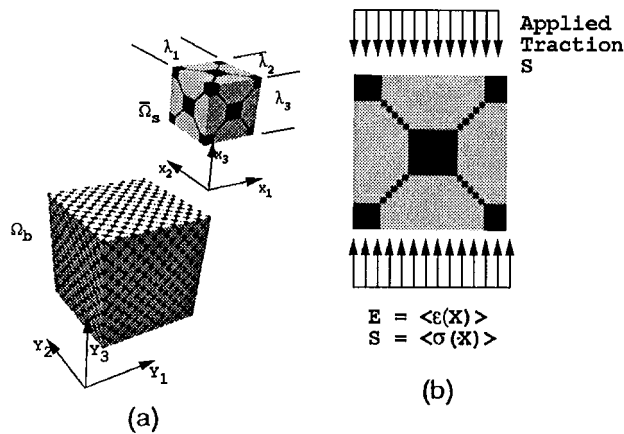


Figure 1. (a) Unit cell  $\tilde{\Omega}_s$  isolated from a composite structure  $\Omega_B$  having a periodic material structure with wave-lengths  $\lambda_1, \lambda_2, \lambda_3$ . (b) Schematic of numerical homogenization experiment performed on the unit cell  $\tilde{\Omega}_s$  to obtain effective stress-strain ( $\mathbf{S}$ - $\mathbf{E}$ ) responses and to compute the local fields  $\boldsymbol{\sigma}(\mathbf{X})$  and  $\boldsymbol{\varepsilon}(\mathbf{X})$

arises primarily because the functional forms of effective medium constitutive models for composites with inelastic constituents are considerably more complex than those of linear anisotropic elasticity and are very difficult to determine. For example, even in the relatively simple case of a two-phased composite where one phase is linear, isotropic and elastic, and the second phase is isotropic and elastic-perfectly-plastic, the macroscopic stress-strain response of the composite will generally feature anisotropy of both strength and stiffness and gradual hardening plasticity behaviour<sup>12, 25</sup> due to the spatial variation in onset of local yielding behaviour on the microscale. With general inelastic constituents there is no fixed relationship between the applied macroscopic strains  $E_{kl}$  and the local strain field  $\varepsilon_{kl}(\mathbf{X})$  as there is for linear elastic composites, and the local incremental compliance of the material located at each point  $\mathbf{X}$  in the unit cell can vary with such quantities such as local stress magnitude, loading rate, and history variables. As a result, even simple two-phased composites, where only one phase has non-linear inelastic behaviour, can potentially behave as if comprised of an infinite number of similar materials. This has been noted previously in References 24 and 25 and is reflected in part in the constitutive modelling techniques used by some investigators.<sup>29</sup> As a result, one can only guess at the appropriate functional form of constitutive models for composites involving inelastic constituents, and such guesses usually provide only gross approximations.<sup>30</sup>

### 1.3. Structural topology formulation based on simplified mixing rules

In light of the difficulties associated with constitutive modelling of inelastic composites, the extension of structural topology optimization frameworks based on homogenization methods to applications involving general combinations of inelastic materials appears to be quite challenging. Two classical and very approximate simplifications to unit cell homogenization methods are those proposed by Voigt<sup>31</sup> and Reuss.<sup>32</sup> In Voigt's simplification, the strain field  $\boldsymbol{\varepsilon}(\mathbf{X})$  throughout the unit cell is assumed to be uniform and equal to that of an applied macro strain  $\mathbf{E}$ , whereas in Reuss's simplification, the stress field  $\boldsymbol{\sigma}(\mathbf{X})$  throughout the composite is assumed to be uniform and equal to that of an applied macrostress  $\mathbf{S}$ . Under these approximate but greatly simplified models,

the microstress and microstrain fields in the composite are fully determined by the assumptions being applied. For example, under the Voigt assumption, application of a macroscopic strain state  $\boldsymbol{\varepsilon}(\mathbf{X}) = \mathbf{E}$  to the composite leads to the macroscopic stress state

$$\mathbf{S}_{\text{Voigt}} = \phi_{\mathcal{A}} \boldsymbol{\sigma}_{\mathcal{A}}(\mathbf{E}) + \phi_{\mathcal{B}} \boldsymbol{\sigma}_{\mathcal{B}}(\mathbf{E}) \quad (3)$$

where  $\phi_{\mathcal{A}}$  and  $\phi_{\mathcal{B}}$  represent the respective volume fractions of materials  $\mathcal{A}$  and  $\mathcal{B}$  in the composite. Under the Reuss assumption, application of a uniform stress state  $\boldsymbol{\sigma}(\mathbf{X}) = \mathbf{S}$  to the composite leads to the following macroscopic strain state:

$$\mathbf{E}_{\text{Reuss}} = \phi_{\mathcal{A}} \boldsymbol{\varepsilon}_{\mathcal{A}}(\mathbf{S}) + \phi_{\mathcal{B}} \boldsymbol{\varepsilon}_{\mathcal{B}}(\mathbf{S}) \quad (4)$$

In the preceding expressions,  $(\boldsymbol{\varepsilon}_{\mathcal{A}}, \boldsymbol{\varepsilon}_{\mathcal{B}})$ ,  $(\boldsymbol{\sigma}_{\mathcal{A}}, \boldsymbol{\sigma}_{\mathcal{B}})$  represent, respectively, the strain and stress states in material phases  $\mathcal{A}$  and  $\mathcal{B}$ . Due to the relative simplicity of these forms for obtaining the effective stress–strain relationships for mixtures of inelastic materials, they are potentially very attractive for usage in structural topology optimization computations.

A number of features of the classical Voigt and Reuss assumptions are well-recognized:

1. They do not in any way provide accurate constitutive material models for composites, but rather only loose upper (Voigt) and lower (Reuss) bounds on the stiffness behaviours of composites.
2. In a strict sense, composites which satisfy either the Voigt or Reuss assumptions are not physically realizable since the Voigt assumption leads to a local stress field that cannot be in equilibrium, and the Reuss assumption leads to a local displacement field that cannot satisfy compatibility requirements.

While the Voigt and Reuss mixing rules are not physically realizable, it is worth noting that many of the microstructures used in alternative topology frameworks are not practically manufacturable due to materials science and processing constraints. Since the objective of this effort is to investigate a topology optimization framework that will employ mixtures or composites only in intermediate design states and which will be virtually free of such mixtures in the final design, these non-realizable features of the Voigt and Reuss simplifications are acceptable.

#### 1.4. Scope

The topology formulation under study in this paper will therefore describe general mixtures of materials physically in terms of the volume fractions of the material phases present, and will use hybrid combinations of the classical Voigt and Reuss mixing rules to describe the gross features of their constitutive behaviours. In the body of this paper, algorithms are derived for the numerical integration of the incremental constitutive equations of a Reuss mixture of two general, isotropic solids and a Voigt mixture of two general, isotropic solids. The algorithms effectively create approximate incremental constitutive models for the local mixtures at the FEM spatial integration points. The macroscopic constitutive behaviours of the mixtures are based on the incremental constitutive behaviours of the individual material phases present, which naturally depend upon their local loading and deformation histories. The perceived utility of this approach is that general materials can be combined algorithmically to obtain usable stress–strain relations in structural analysis calculations without the necessity of devising appropriate functional forms for the constitutive models of mixtures and describing the variation of the free parameters in such models with the variation of design variables such volume fractions and microstructural parameters. The

proposed approach being studied may provide one feasible avenue for extending topology design methods to important classes of problems involving inelastic materials.

Having selected a method for characterizing approximate constitutive behaviours of material mixtures, a structural topology optimization formulation that addresses non-linear material behaviours is developed using non-linear structural analysis techniques. Furthermore, since optimal topology solutions are to be obtained with gradient-based optimization techniques, accurate and efficient design sensitivity analysis methods are required. In previous works on *shape* design of structures involving non-linear, inelastic materials, adjoint sensitivity methods have been investigated by Arora and Lee<sup>33</sup> and direct differentiation methods have been implemented and studied by Ohsaki and Arora<sup>34</sup> and Haber and Vidal.<sup>35</sup> Here, direct differentiation techniques are developed for sensitivity analysis of generalized compliance with respect to the topology of structural systems. The proposed design sensitivity expressions are valid for general materially non-linear structures that remain within the geometrically linear regime of behaviour.

The remainder of this paper is organized as follows. In Section 2 a microstructure free framework for describing the distribution of material phases (including mixtures) throughout a fixed spatial design domain is briefly reviewed. Section 3 formulates structural topology problems where mixtures of general non-linear materials are involved, and develops incremental design sensitivity algorithms based on direct differentiation methods. Integration algorithms for mixtures of general inelastic materials in a small-strain framework are developed in Section 4 for both the Voigt and Reuss assumptions. The consistency between the proposed Voigt–Reuss topology formulation and the proposed design sensitivity analysis methods is established in Section 5 and the methods are demonstrated on two sample computations involving optimization of structural topology to maximize a structure's ultimate strength. The general performance of the new mixing algorithms and design sensitivity analysis algorithms are assessed in Section 6 and specific areas requiring further investigation are discussed.

## 2. DISTRIBUTION OF MATERIALS

In the following development, the complete undeformed spatial domain of the structure being designed is denoted by  $\Omega_S$ ; its designable subset by  $\Omega_D$ ; and its non-designable subset in which the spatial/topological arrangement of materials is taken to be fixed by  $\Omega_N$ . The arrangement of  $N$  pre-selected candidate materials in  $\Omega_D$  remains to be determined and so this region is called *designable*. A set of single or multiple loading/boundary conditions to which  $\Omega_S$  will be subjected are specified and a starting design  $\mathbf{b}^{(0)}$  which specifies the initial material layout in the  $\Omega_D$  is selected. For each set of loading/boundary conditions, the structure is analysed as a boundary value problem.

Since the design of the structure is considered to be the spatial distribution of the  $N$  candidate materials throughout the spatially fixed design domain  $\Omega_D$ , a system is needed to describe the material distributions. For the discrete two-material layout problem involving material  $\mathcal{A}$  and material  $\mathcal{B}$ , the binary indicator function describing the arrangement of material  $\mathcal{A}$  would be

$$\chi_{\mathcal{A}}(\mathbf{X}) = \begin{cases} 1 & \text{if material } \mathcal{A} \text{ fully occupies point } \mathbf{X} \in \Omega_D \\ 0 & \text{otherwise} \end{cases} \quad (5)$$

while that for material  $\mathcal{B}$  would be

$$\chi_{\mathcal{B}}(\mathbf{X}) = \begin{cases} 1 & \text{if material } \mathcal{B} \text{ fully occupies point } \mathbf{X} \in \Omega_{\mathcal{D}} \\ 0 & \text{otherwise} \end{cases} \quad (6)$$

The respective domains  $\Omega_{\mathcal{A}}$  and  $\Omega_{\mathcal{B}}$  occupied by materials  $\mathcal{A}$  and  $\mathcal{B}$  would simply be

$$\Omega_{\mathcal{A}} = \{\mathbf{X} \in \Omega_{\mathcal{D}} | \chi_{\mathcal{A}}(\mathbf{X}) = 1; \chi_{\mathcal{B}}(\mathbf{X}) = 0\} \quad (7a)$$

$$\Omega_{\mathcal{B}} = \{\mathbf{X} \in \Omega_{\mathcal{D}} | \chi_{\mathcal{B}}(\mathbf{X}) = 1; \chi_{\mathcal{A}}(\mathbf{X}) = 0\} \quad (7b)$$

Preference is given here to discrete final material distributions that satisfy  $\Omega_{\mathcal{A}} \cap \Omega_{\mathcal{B}} = \emptyset$  and  $\Omega_{\mathcal{A}} \cup \Omega_{\mathcal{B}} = \Omega_{\mathcal{D}}$ . These distributions are achieved, however, through continuous formulations which permit *mixtures* to exist throughout the design domain  $\Omega_{\mathcal{D}}$ . By permitting mixtures, the material phases  $\mathcal{A}$  and  $\mathcal{B}$  are allowed to simultaneously and partially occupy an infinitesimal neighbourhood about each spatial point  $\mathbf{X}$  in  $\Omega_{\mathcal{D}}$ . In describing the mixtures, the binary indicator functions above are no longer useful, but a straightforward and continuous generalization of the binary indicator function concept is available using the volume fraction concept. As employed here the volume fraction of material phase  $\mathcal{A}$  at a fixed spatial point  $\mathbf{X}$  in the design domain  $\Omega_{\mathcal{D}}$  is denoted by  $\phi_{\mathcal{A}}(\mathbf{X})$  and represents *the fraction of an infinitesimal volume element surrounding point  $\mathbf{X}$  occupied by material  $\mathcal{A}$* . The volume fraction definition for material phase  $\mathcal{B}$  and others is similar. Natural constraints upon the spatial volume fractions for the two-material problem are

$$0 \leq \phi_{\mathcal{A}}(\mathbf{X}) \leq 1, \quad 0 \leq \phi_{\mathcal{B}}(\mathbf{X}) \leq 1, \quad \phi_{\mathcal{A}}(\mathbf{X}) + \phi_{\mathcal{B}}(\mathbf{X}) = 1 \quad (8)$$

The last physical constraint of (8) states that the material volume fractions at  $\mathbf{X}$  are not independent. Thus in two-material problems as treated in this paper, one need only be concerned with the layout of phase  $\mathcal{A}$  since that of phase  $\mathcal{B}$  follows directly from (8)<sub>3</sub>. The volume fraction method of describing material distributions neither relies upon nor assumes a microstructure or morphology of the local mixture and is a very straightforward generalization of the binary indicator function approach.

In the proposed topology design optimization framework, the design domain  $\Omega_{\mathcal{D}}$  will be discretized into NEL low-order finite elements such as bilinear continuum degenerated shell elements or trilinear three-dimensional continuum elements. For these low-order elements, the independent material volume fraction  $\phi_{\mathcal{A}}$  is taken as piecewise constant over the spatial domain occupied by individual finite elements. The designable spatial/topological distribution of material phase  $\mathcal{A}$  in  $\Omega_{\mathcal{D}}$  can thus be described by a vector of design variables  $\mathbf{b}$  with contributions from each element comprising  $\Omega_{\mathcal{D}}$ . Specifically, the design vector  $\mathbf{b}$  has the definition:

$$\mathbf{b} := \{\phi_{\mathcal{A}_1}, \phi_{\mathcal{A}_2}, \dots, \phi_{\mathcal{A}_{NEL}}\} \quad (9)$$

That is, the full vector of design variables  $\mathbf{b}$  is comprised of NEL scalar-valued element level contributions  $\phi_{\mathcal{A}_i}$ , each of which represents the volume fraction of phase  $\mathcal{A}$  in the  $i$ th element. This system allows the two candidate materials to be arbitrarily distributed throughout the NEL finite elements comprising the design domain  $\Omega_{\mathcal{D}}$ , subject only to natural constraints such as  $\sum_{j=1}^2 \phi_{ij} = 1$ , for each  $i \in \{1, 2, \dots, NEL\}$  and  $\phi_{ij} \in [0, 1]$  for  $j \in \{1, 2\}$ .

*Remark 2.1.* It is recognized that compliance minimization topology formulations using bilinear (or trilinear) interpolation of displacement fields and material distribution layout design parameters

that are uniform over individual element domains are unstable in that they generally yield mesh-dependent, checkerboarding designs.<sup>36, 37</sup> This instability problem can be easily rectified, however, using the spatial filtering techniques proposed in Reference 18, so that stable material layout designs can be achieved with low-order elements.

Global material cost constraints are generally imposed upon the designed structure by specifying appropriate upper or lower limits on the global volume fraction of the independent material phase. A typical upper bound for a solid phase is represented as  $\langle \phi_{\mathcal{A}} \rangle - C_{\mathcal{A}} \leq 0$ , where  $C_{\mathcal{A}}$  is a designer specified upper bound value on the global volume fraction of material phase  $\mathcal{A}$  in the structural domain  $\Omega_S$ . The global volume fraction of phase  $\mathcal{A}$  over the structural domain is calculated as

$$\langle \phi_{\mathcal{A}} \rangle = \frac{\int_{\Omega_S} \phi_{\mathcal{A}}(\mathbf{X}) \, d\Omega_S}{\int_{\Omega_S} d\Omega_S} \quad (10)$$

### 3. THE TOPOLOGY DESIGN FORMULATION

#### 3.1. Objective and constraint functionals

Numerous formulation options exist in structural and composite material topology design optimization via utilization of assorted combinations of objective and constraint functionals, and the framework advanced here accommodates these alternatives. All design optimization formulations involve specification of an objective functional and a number of constraint functionals which can be of either equality or inequality type. In the proposed formulation, the design variables are continuous and real-valued and it is assumed that the associated functionals, both objective and constraints, will also be continuous and real-valued as well as piecewise differentiable.

Within the realm of continuous real-valued functionals  $\mathcal{F}$  it is helpful to distinguish between purely cost based functionals which are *independent* of the response of the system being designed (that is  $\mathcal{F} = \mathcal{F}(\mathbf{b})$ ) and performance based functionals which by definition depend upon *both* the design variables  $\mathbf{b}$  and the performance or state of the designed system which can generally be described in terms of  $\mathbf{u}$ , the vector displacement field (that is  $\mathcal{F} = \mathcal{F}(\mathbf{b}, \mathbf{u})$ ). To demonstrate, an example of a pure *cost* functional for the structural topology optimization problem is the overall volume fraction of one of the candidate constituent phases, which can be specified as

$$\mathcal{F}_{\phi_{\mathcal{A}}} = \langle \phi_{\mathcal{A}} \rangle - C_{\mathcal{A}} \quad (11)$$

in which  $\langle \phi_{\mathcal{A}} \rangle$  represents the volume average of  $\phi_{\mathcal{A}}$  over the entire design domain  $\Omega_D$ . In contrast, the global strain energy functional over the structural domain for general loading conditions would be defined as

$$\mathcal{F}_E = \int_0^t \int_{\Omega_S} \boldsymbol{\sigma} : \dot{\boldsymbol{\epsilon}} \, d\Omega_S \, d\tau \quad (12)$$

where  $\tau$  is a parametric time variable. The strain energy functional is clearly dependent upon both the design variables  $\mathbf{b}$  and the related performance of the system  $\mathbf{u}$ . A typical topology design optimization problem to minimize generalized compliance might be to minimize the strain energy  $\mathcal{F}_E$  in a structure undergoing a prescribed, force-controlled loading programme, thereby maximizing

the stiffness of the structure under the applied loading, subject to a volume constraint on one of the material phases. An equally viable alternative formulation of the generalized compliance minimization problem would be to maximize the strain energy  $\mathcal{F}_E$  in a structure undergoing loading from a programme of prescribed displacements, again with an upper bound constraint on one of the material phases.

The topology design optimization process is iterative in nature, requiring the solution of one or more analysis problems with each new variation of the design. Intermingled with solving the analysis problem(s) is the evaluation of the objective and constraint functionals as well as their design gradients. The following two subsections formulate the general analysis and design sensitivity analysis problems.

### 3.2. The analysis problem

Topology design can be performed to find the optimal layout of a structure to: minimize compliance; maximize strength; tailor eigenvalues; and tune dynamic response. These varied objectives require the solution of elliptic boundary value problems; eigenvalue problems; and hyperbolic initial and boundary value problems. While the framework under study here can and does include all of these classes of problems, attention is restricted here to the class of problems requiring solution of quasi-static material non-linear elliptic boundary value problems, which naturally recover linearity as a special case.

The strong form of the general material non-linear elliptic boundary value problem to be solved is: Find  $\mathbf{u}: (\Omega_S \times [0, T]) \mapsto \mathbb{R}^3$  such that

$$\sigma_{ij,i} + \rho\gamma_j = 0 \text{ on } \Omega_S \quad \forall t \in [0, T] \quad (13a)$$

subject to the boundary conditions:

$$u_j(t) = g_j(t) \quad \text{on } \Gamma_{g_j} \text{ for } j = 1, 2, 3, \quad t \in [0, T] \quad (13b)$$

$$n_i \sigma_{ij} = h_j(t) \quad \text{on } \Gamma_{h_j} \text{ for } j = 1, 2, 3, \quad t \in [0, T] \quad (13c)$$

As is customary, it is assumed that the surface  $\Gamma$  of the structural domain  $\Omega_S$  admits the decomposition  $\Gamma = \overline{\Gamma_{g_j}} \cup \overline{\Gamma_{h_j}}$  and  $\Gamma_{g_j} \cap \Gamma_{h_j} = \emptyset$ , for  $j = 1, 2, 3$ .

Since the analysis problem is being solved in the context of topology optimization, it is assumed that a local microscopic mixture of two generic materials  $\mathcal{A}$  and  $\mathcal{B}$  resides at each point  $\mathbf{X}$  in the structural domain  $\Omega_S$ . In equation (13a)  $\sigma$  thus represents the macroscopic stress of the local mixture which is dependent upon the constitutive properties of the two material phases and the mixing rule employed

$$\sigma(\mathbf{X}) = \sigma[\sigma^{\mathcal{A}}(\boldsymbol{\varepsilon}^{\mathcal{A}}, \dot{\boldsymbol{\varepsilon}}^{\mathcal{A}}, \boldsymbol{\zeta}^{\mathcal{A}}); \sigma^{\mathcal{B}}(\boldsymbol{\varepsilon}^{\mathcal{B}}, \dot{\boldsymbol{\varepsilon}}^{\mathcal{B}}, \boldsymbol{\zeta}^{\mathcal{B}}); (\phi_{\mathcal{A}}, \phi_{\mathcal{B}})] \quad (14)$$

Detailed algorithmic treatment of the mixing rules in accordance with the Voigt and Reuss assumptions is provided in Section 4 and includes a decomposition of the local macroscopic strain  $\boldsymbol{\varepsilon} = \nabla^s \mathbf{u}$  into strains  $\boldsymbol{\varepsilon}^{\mathcal{A}}$  and  $\boldsymbol{\varepsilon}^{\mathcal{B}}$  for the respective material phases. The mass density  $\rho$  of the local mixture is simply  $\rho = \phi_{\mathcal{A}} \rho_{\mathcal{A}} + \phi_{\mathcal{B}} \rho_{\mathcal{B}}$ .

The weak or variational form of the problem is obtained by restating the strong form as

$$\int_{\Omega_S} [\sigma_{ij,i} \delta u_j + \rho \gamma_j \delta u_j] d\Omega_S = 0 \quad (15)$$

from which integration by parts, usage of Green's Theorem and utilization of the natural boundary conditions gives the virtual work equation

$$\int_{\Omega_S} \sigma_{ij} \delta \varepsilon_{ij} \, d\Omega_S = \int_{\Omega_S} \rho \gamma_j \delta u_j \, d\Omega_S + \int_{\Gamma_h} h_j \delta u_j \, d\Gamma_h. \quad (16)$$

Usage of a Galerkin formulation in which the real and variational kinematic fields are expanded in terms of the same nodal basis functions, and discretization of the time domain into a finite number of discrete time points, leads to the following force balance equations at each unrestrained node A in the mesh as here at the  $(n + 1)$ th time step:

$$(\mathbf{r}_A)_{n+1} = (\mathbf{f}_A^{\text{int}})_{n+1} - (\mathbf{f}_A^{\text{ext}})_{n+1} = \mathbf{0} \quad (17)$$

where

$$(\mathbf{f}_A^{\text{int}})_{n+1} = \int_{\Omega_S} \mathbf{B}_A^T : \boldsymbol{\sigma}_{n+1} \, d\Omega_S \quad (18a)$$

$$(\mathbf{f}_A^{\text{ext}})_{n+1} = \int_{\Omega_S} \rho N_A \gamma_{n+1} \, d\Omega_S + \int_{\Gamma_h} N_A \mathbf{h}_{n+1} \, d\Gamma_h \quad (18b)$$

In (18),  $\mathbf{B}_A$  represents the nodal strain displacement matrix ( $\mathbf{B}_A = \nabla^s N_A(\mathbf{x})$ ), and  $N_A$  denotes the nodal basis function for the  $A$ th node. In general, (17) represents a set of non-linear algebraic equations which must be solved in an iterative fashion for the incremental displacement field  $(\Delta \mathbf{u})_{n+1} = \mathbf{u}_{n+1} - \mathbf{u}_n$  for each time step of the analysis problem. Numerous options exist for solving non-linear systems such as (17), a few of which are reviewed in detail in Reference 12.

### 3.3. Design sensitivity analysis algorithms

Energy-based functionals to minimize the generalized compliance of structures are here considered to be of the form

$$\Pi(t) = \int_0^t \int_{\Gamma_h} \mathbf{h}(\tau) \cdot \dot{\mathbf{u}} \, d\Gamma_h \, d\tau + \int_0^t \int_{\Omega_S} \rho \gamma(\tau) \cdot \dot{\mathbf{u}} \, d\Omega_S \, d\tau - \int_0^t \int_{\Gamma_g} \mathbf{n} \cdot \boldsymbol{\sigma} \cdot \dot{\mathbf{g}}(\tau) \, d\Gamma_g \, d\tau \quad (19)$$

Generalized compliance functionals  $\Pi$  which quantify the work done by external agencies on the structural domain  $\Omega_S$  can be separated into work terms resulting solely from applied external traction forces  $\mathbf{h}(\tau)$  and body forces  $\rho \gamma(\tau)$ , and work terms resulting solely from applied displacements  $\mathbf{g}(\tau)$ . In structural topology optimization of linear elastic structures, the case most often considered has been that of prescribed external force type loadings. For inelastic structures, however, such force-controlled structural analysis problems are potentially ill-posed (solutions of Eq. (17) may not exist), and so formulations for structures loaded by displacements must also be considered. In the following, it is assumed for simplicity of presentation that the structures being designed are loaded either by applied external traction and/or body forces or by prescribed, non-vanishing displacements. Sensitivity analysis algorithms for the generalized compliance functional (19) are developed independently in the following two subsections for force-type loadings (Section 3.3.1) and for displacement-type loadings (Section 3.3.2). For the more general case of structures acted upon simultaneously by both types of loadings, the DSA results for the special subcases can be straightforwardly combined.

3.3.1. *Generalized compliance DSA for force-loaded structures.* For structures subjected only to external force type loadings, the generalized compliance functionals to be treated can be evaluated incrementally each time step of the analysis problem as

$$\mathcal{F}_E(t_N) = \mathcal{F}_E(t_0) + \sum_{n=1}^N (\Delta \mathcal{F}_E)_n \quad (20)$$

where

$$(\Delta \mathcal{F}_E)_{n+1} = \frac{1}{2}(\mathbf{f}_n^{\text{ext}} + \mathbf{f}_{n+1}^{\text{ext}}) \cdot (\Delta \mathbf{u})_{n+1} = \mathbf{f}_{n+\frac{1}{2}}^{\text{ext}} \cdot (\Delta \mathbf{u})_{n+1} \quad (21)$$

In calculating the total design derivative of the energy functional (20) it will be assumed that  $\mathcal{F}_E(t_0)$  either vanishes or is independent of the design state  $\mathbf{b}$ . Thus to calculate the design gradient of (20) one needs only to sum the design gradients of the incremental energy contributions given by (21). The design gradient of the incremental energy functionals under external force loadings takes the form

$$\frac{d(\Delta \mathcal{F}_E)_{n+1}}{d\mathbf{b}} = \frac{\partial(\mathbf{f}_{n+\frac{1}{2}}^{\text{ext}})}{\partial \mathbf{b}} \cdot (\Delta \mathbf{u})_{n+1} + (\mathbf{f}_{n+\frac{1}{2}}^{\text{ext}}) \cdot \frac{d(\Delta \mathbf{u})_{n+1}}{d\mathbf{b}} \quad (22)$$

While the first term on the right-hand side of (22) is quite simple to calculate, the second term is somewhat more involved and requires extra precautions in the calculation of  $[d(\Delta \mathbf{u})_{n+1}]/d\mathbf{b}$ .

At the generic  $(n+1)$ th time step the analysis problem moves from the equilibrium state  $\mathbf{r}_n = \mathbf{0}$  to the equilibrium state  $\mathbf{r}_{n+1} = \mathbf{0}$ . Since the equilibrium state is assumed to be satisfied at all time steps, irrespective of the design state  $\mathbf{b}$ , we can designate the *incremental* state equation as

$$\Delta \mathbf{r}_{n+1} = \mathbf{r}_{n+1} - \mathbf{r}_n = \mathbf{0} \quad (23)$$

which for the case of the material non-linear, but geometrically linear, analysis problems under consideration takes the form:

$$\Delta \mathbf{r}_{n+1} = \int_{\Omega_S} \mathbf{B}^T : (\boldsymbol{\sigma}_{n+1} - \boldsymbol{\sigma}_n) d\Omega_S - (\mathbf{f}_{n+1}^{\text{ext}} - \mathbf{f}_n^{\text{ext}}) \quad (24a)$$

$$= \int_{\Omega_S} \mathbf{B}^T : \Delta \boldsymbol{\sigma}_{n+1} d\Omega_S - \Delta \mathbf{f}_{n+1}^{\text{ext}} \quad (24b)$$

If general inelastic material behaviours are assumed, the local stress update at a specific integration point in  $\Omega_S$  has a fading memory of all previous stress and strain states at this same point and will thus be of the general form:  $\Delta \boldsymbol{\sigma}_{n+1} = \Delta \boldsymbol{\sigma}_{n+1}(\mathbf{b}; \boldsymbol{\sigma}_n; \boldsymbol{\varepsilon}_n; \Delta \boldsymbol{\varepsilon}_{n+1})$ . For general constitutive models having this form of algorithmic stress update, the complete design derivative of the stress increment takes the form

$$\begin{aligned} \frac{d\Delta \boldsymbol{\sigma}_{n+1}}{d\mathbf{b}} &= \frac{\partial \Delta \boldsymbol{\sigma}_{n+1}}{\partial \mathbf{b}} + \frac{\partial \Delta \boldsymbol{\sigma}_{n+1}}{\partial \boldsymbol{\varepsilon}_n} \frac{\partial \boldsymbol{\varepsilon}_n}{\partial \mathbf{u}_n} \frac{d\mathbf{u}_n}{d\mathbf{b}} + \frac{\partial \Delta \boldsymbol{\sigma}_{n+1}}{\partial \boldsymbol{\sigma}_n} \frac{d\boldsymbol{\sigma}_n}{d\mathbf{b}} \\ &+ \frac{\partial \Delta \boldsymbol{\sigma}_{n+1}}{\partial \Delta \boldsymbol{\varepsilon}_{n+1}} \frac{\partial \Delta \boldsymbol{\varepsilon}_{n+1}}{\partial \Delta \mathbf{u}_{n+1}} \frac{d\Delta \mathbf{u}_{n+1}}{d\mathbf{b}} \end{aligned} \quad (25a)$$

$$= \frac{\partial \Delta \boldsymbol{\sigma}_{n+1}}{\partial \mathbf{b}} + \mathbf{Z}_{n+1} : \mathbf{B} \cdot \frac{d\mathbf{u}_n}{d\mathbf{b}} + \mathbf{Y}_{n+1} : \frac{d\boldsymbol{\sigma}_n}{d\mathbf{b}} + \mathbf{C}_{n+1} : \mathbf{B} \cdot \frac{d\Delta \mathbf{u}_{n+1}}{d\mathbf{b}} \quad (25b)$$

where

$$\mathbf{Y}_{n+1} \equiv \frac{\partial \Delta \boldsymbol{\sigma}_{n+1}}{\partial \boldsymbol{\sigma}_n}, \quad \mathbf{Z}_{n+1} \equiv \frac{\partial \Delta \boldsymbol{\sigma}_{n+1}}{\partial \boldsymbol{\varepsilon}_n}, \quad \mathbf{C}_{n+1} \equiv \frac{\partial \Delta \boldsymbol{\sigma}_{n+1}}{\partial \Delta \boldsymbol{\varepsilon}_{n+1}} \quad (26)$$

Accordingly, differentiation of the incremental equilibrium state equation at the end of the  $(n+1)$ th time step yields:

$$\mathbf{0} = \frac{d\Delta \mathbf{r}_{n+1}}{d\mathbf{b}} \quad (27a)$$

$$\begin{aligned} &= \int_{\Omega_S} \mathbf{B}^T : \frac{\partial \Delta \boldsymbol{\sigma}_{n+1}}{\partial \mathbf{b}} d\Omega_S + \int_{\Omega_S} \mathbf{B}^T : \mathbf{Y}_{n+1} : \frac{d\boldsymbol{\sigma}_n}{d\mathbf{b}} d\Omega_S \\ &+ \int_{\Omega_S} \mathbf{B}^T : \mathbf{Z}_{n+1} : \mathbf{B} d\Omega_S \cdot \frac{d\mathbf{u}_n}{d\mathbf{b}} + \int_{\Omega_S} \mathbf{B}^T : \mathbf{C}_{n+1} : \mathbf{B} d\Omega_S \cdot \frac{d(\Delta \mathbf{u})_{n+1}}{d\mathbf{b}} - \frac{\partial \Delta \mathbf{f}_{n+1}^{\text{ext}}}{\partial \mathbf{b}} \end{aligned} \quad (27b)$$

*Remark 3.1.*  $\mathbf{C}_{n+1}$  in (26) and (27b) is the generalization of the consistent tangent operator<sup>38</sup> for the local mixture of materials to be discussed in Section 4. In non-linear sensitivity analysis, it has been previously noted,<sup>35</sup> that the maintenance of accuracy in sensitivity results, especially with sizable load increments, is vitally dependent upon the usage of such tangent operators which are *consistent* with the integration algorithms for the constitutive models being employed.

The expressions in (27b) can be inverted to obtain  $[d(\Delta \mathbf{u})_{n+1}]/d\mathbf{b}$  as

$$\begin{aligned} \frac{d(\Delta \mathbf{u})_{n+1}}{d\mathbf{b}} &= -[\mathbf{K}_{n+1}]^{-1} \left[ \int_{\Omega_S} \mathbf{B}^T : \frac{\partial \Delta \boldsymbol{\sigma}_{n+1}}{\partial \mathbf{b}} d\Omega_S + \int_{\Omega_S} \mathbf{B}^T : \mathbf{Y}_{n+1} : \frac{d\boldsymbol{\sigma}_n}{d\mathbf{b}} d\Omega_S \right. \\ &\left. + \int_{\Omega_S} \mathbf{B}^T : \mathbf{Z}_{n+1} : \mathbf{B} d\Omega_S \cdot \frac{d\mathbf{u}_n}{d\mathbf{b}} - \frac{\partial \Delta \mathbf{f}_{n+1}^{\text{ext}}}{\partial \mathbf{b}} \right] \end{aligned} \quad (28)$$

where  $\mathbf{K}_{n+1}$  is the tangent stiffness operator for the incremental structural analysis problem evaluated with the converged displacement field following the  $(n+1)$ th time step. The result of (28) is employed in (22) to complete the gradient calculation of the incremental energy function. In those classes of problems where it is actually necessary to compute and maintain the design gradient of the displacement vector  $d\mathbf{u}/d\mathbf{b}$ , the result of (28) must also be used to update the design gradient of the displacement vector  $\mathbf{u}_{n+1}$  for usage in subsequent DSA operations:

$$\frac{d\mathbf{u}_{n+1}}{d\mathbf{b}} = \frac{d\mathbf{u}_n}{d\mathbf{b}} + \frac{d(\Delta \mathbf{u})_{n+1}}{d\mathbf{b}} \quad (29)$$

In addition, the design gradient of the stress at each integration point is then updated according to (25). It is thus quite clear that variable topology design sensitivity analysis with general inelastic materials is potentially quite involved, generally requiring computation and storage of  $d\mathbf{u}/d\mathbf{b}$  at the nodes where external forces are applied, and computation/storage of  $d\boldsymbol{\sigma}/d\mathbf{b}$  in those elements having nodes at which external forces are applied. Given the large number of design variables employed in topology optimization, the required computational effort and memory can be considerable

depending upon the complexity of the loading pattern. For certain classes of materials, however, it will not be necessary to compute or store either of these quantities, leading to considerable savings.

*3.3.1.1. Special case 1: linear elastic structures.* In structures of linear elastic materials the form of the stress update equation throughout  $\Omega_S$  will be  $\sigma_{n+1} = \sigma_n + \mathbf{E}(\mathbf{b}) : \Delta \varepsilon_{n+1}$ . When the constitutive equation is of this simple form, then (28) reduces to

$$\frac{d(\Delta \mathbf{u})_{n+1}}{d\mathbf{b}} = -\mathbf{K}^{-1} \cdot \frac{\partial \Delta \mathbf{r}_{n+1}}{\partial \mathbf{b}} = -\mathbf{K}^{-1} \cdot \left[ \int_{\Omega_S} \mathbf{B}^T : \frac{\partial(\Delta \sigma)_{n+1}}{\partial \mathbf{b}} d\Omega_S - \frac{\partial \Delta \mathbf{f}_{n+1}^{\text{ext}}}{\partial \mathbf{b}} \right] \quad (30)$$

Accordingly, (22) can thus be re-written in the particularly simple form, making usage of (30):

$$\frac{d(\Delta \mathcal{F}_E)_{n+1}}{d\mathbf{b}} = \frac{\partial \mathbf{f}_{n+1/2}^{\text{ext}}}{\partial \mathbf{b}} \cdot \Delta \mathbf{u}_{n+1} + \mathbf{u}_{n+1}^a \cdot \frac{\partial \Delta \mathbf{r}_{n+1}}{\partial \mathbf{b}} \quad (31)$$

where  $\mathbf{u}_{n+1}^a = -\mathbf{K}^{-1} \cdot \mathbf{f}_{n+1/2}^{\text{ext}}$ . Thus for the case of linear elastic structures it is not necessary to explicitly calculate or store either of the total derivative quantities  $d\mathbf{u}/d\mathbf{b}$  or  $d\sigma/d\mathbf{b}$ .

*3.3.1.2. Special case 2: structures of inviscid elastoplastic materials.* In structures of inviscid elastoplastic materials where the elasticity tensor is constant, the form of the stress update equation at each integration point can be written

$$\Delta \sigma_{n+1} = \mathbf{E} : (\Delta \varepsilon_{n+1} - \Delta \varepsilon_{n+1}^P) \quad (32)$$

where  $\mathbf{E}$  is the effective elasticity tensor for the local mixture of materials and  $\Delta \varepsilon_{n+1}^P$  is the plastic strain increment for the mixture. Using generalized consistent tangent operators<sup>38</sup> the *linearized* form of this update equation can be written simply as

$$\Delta \sigma_{n+1} \doteq \mathbf{C}_{n+1} : \Delta \varepsilon_{n+1} \quad (32)$$

where  $\mathbf{C}_{n+1}$  is the effective consistent tangent operator for the local mixture of elastoplastic materials. When the linearized incremental constitutive equation is of this simple form, then (28) reduces to

$$\frac{d(\Delta \mathbf{u})_{n+1}}{d\mathbf{b}} = -[\mathbf{K}_{n+1}]^{-1} \cdot \left[ \int_{\Omega_S} \mathbf{B}^T : \frac{\partial \Delta \sigma_{n+1}}{\partial \mathbf{b}} d\Omega_S - \frac{\partial(\Delta \mathbf{f}_{n+1}^{\text{ext}})}{\partial \mathbf{b}} \right] \quad (33)$$

Accordingly, (22) can thus be re-written in the particularly simple form, making usage of (33):

$$\frac{d(\Delta \mathcal{F}_E)_{n+1}}{d\mathbf{b}} = \frac{\partial \mathbf{f}_{n+1/2}^{\text{ext}}}{\partial \mathbf{b}} \cdot (\Delta \mathbf{u})_{n+1} + \mathbf{u}_{n+1}^a \cdot \left[ \int_{\Omega_S} \mathbf{B}^T : \frac{\partial \Delta \sigma_{n+1}}{\partial \mathbf{b}} d\Omega_S - \frac{\partial \Delta \mathbf{f}_{n+1}^{\text{ext}}}{\partial \mathbf{b}} \right] \quad (34)$$

where  $\mathbf{u}_{n+1}^a = -\mathbf{K}_{n+1}^{-1} \cdot \mathbf{f}_{n+1/2}^{\text{ext}}$  plays the role of an adjoint displacement field.

*Remark 3.2.* For the special case of force-loaded structures comprised of inviscid, elastoplastic materials, as for linear elastic materials, is not necessary to explicitly calculate or store either of the total derivative quantities  $d\mathbf{u}/d\mathbf{b}$  or  $d\sigma/d\mathbf{b}$ .

*Remark 3.3.* If a strict direct differentiation approach were employed, then the operations suggested by (33) could be quite expensive, since they suggest that *ndesv* additional back-substitution

solutions would need to be obtained in the design sensitivity following each time step, where  $ndesv$  is the number of design variables. For topology optimization,  $ndesv$  can be quite large, suggesting much computational effort. The proposed implementation requires solving only for the adjoint displacement field at each time step, which is much more computationally efficient.

*Remark 3.4.* Force-controlled structural analysis boundary value problems for structures with elastic-perfectly-plastic materials are potentially ill-posed. While such problems can be solved with extra caution required, the strain energy  $\mathcal{F}_E$  is not a convergent quantity as the limit capacity of the structure is reached. An alternative generalized compliance measure which may be of more value in such problems is the complementary strain energy  $\mathcal{F}_C(T) \equiv \int_{t_0}^T \int_{\Omega_S} \boldsymbol{\varepsilon} : \boldsymbol{\sigma} \, d\Omega_S \, dt$ .

3.3.2. *Generalized compliance DSA for displacement-loaded structures.* As an alternative to force-loaded structures, it is sometimes more useful to consider loadings due to the application of prescribed non-vanishing displacements  $\mathbf{g}$  to the structure at a subset of nodes  $\{n_g\}$  comprising the mesh. Such nodes need not necessarily lie on the external boundaries of  $\Omega_S$ , and the associated displacement field is simply  $\mathbf{g} = \sum_{E \in \{n_g\}} N_E(\mathbf{X}) \cdot \mathbf{g}_E$ , where  $\mathbf{g}_E$  are applied nodal displacements. For structures subjected to displacement controlled loading, the incremental energy stored in the structure due to the incremental work done by the applied displacements for the  $(n + 1)$ th time step can be written as

$$(\Delta \mathcal{F}_E)_{n+1} = \int_{t_n}^{t_{n+1}} \int_{\Gamma_g} \mathbf{n} \cdot \boldsymbol{\sigma} \cdot \dot{\mathbf{g}} \, d\Gamma_g \, d\tau \tag{35a}$$

$$= \sum_{E \in \{n_g\}} \Delta \mathbf{g}_{n+1}^E \cdot \left[ \frac{1}{2} \int_{\Omega_S} \mathbf{B}_E^T : (\boldsymbol{\sigma}_n + \boldsymbol{\sigma}_{n+1}) \, d\Omega_S \right] \tag{35b}$$

$$= \sum_{E \in \{n_g\}} \Delta \mathbf{g}_{n+1}^E \cdot (\mathbf{f}_E^{\text{int}})_{n+1/2} \tag{35c}$$

$$= \int_{\Omega_S} \Delta \boldsymbol{\varepsilon}_{n+1}^g : \boldsymbol{\sigma}_{n+1/2} \, d\Omega_S \tag{35d}$$

In the preceding expression,  $\{n_g\}$  represents the set of nodes in the mesh discretization of  $\Omega_S$  at which the prescribed displacements are applied, and at the  $E$ th node in this set,  $\Delta \mathbf{g}_{n+1}^E \equiv \mathbf{g}_{n+1}^E - \mathbf{g}_n^E$ . Also,  $\Delta \boldsymbol{\varepsilon}_{n+1}^g \equiv \sum_{E \in \{n_g\}} \mathbf{B}_E \cdot \Delta \mathbf{g}_{n+1}^E$ . Since  $\Delta \boldsymbol{\varepsilon}_{n+1}^g$  is fully prescribed, the total design gradient of the incremental strain energy takes the form

$$\frac{d(\Delta \mathcal{F}_E)_{n+1}}{d\mathbf{b}} = \int_{\Omega_S} \Delta \boldsymbol{\varepsilon}_{n+1}^g : \frac{d\boldsymbol{\sigma}_{n+1/2}}{d\mathbf{b}} \, d\Omega_S = \sum_{E \in \{n_g\}} \Delta \mathbf{g}_{n+1}^E \cdot \frac{d(\mathbf{f}_E^{\text{int}})_{n+1/2}}{d\mathbf{b}} \tag{36}$$

For the case of general, inelastic materials, expressions for  $d\boldsymbol{\sigma}_n/d\mathbf{b}$  and  $d\Delta \boldsymbol{\sigma}_{n+1}/d\mathbf{b}$  follow from (25). For general classes of materials, it will thus be necessary to compute and store both  $d\boldsymbol{\sigma}/d\mathbf{b}$  and  $d\mathbf{u}/d\mathbf{b}$  in some elements and at the prescribed essential boundary condition nodes. For certain classes of materials, however, this will not always be necessary, as is demonstrated in the two special cases treated below.

3.3.2.1. *Special case 1: linear elastic materials.* In structures comprised entirely of linear elastic materials,  $\sigma_{n+1/2}$  is path independent and can thus be expressed directly as  $\sigma_{n+1/2} = \mathbf{E}(\mathbf{b}) : \boldsymbol{\varepsilon}_{n+1/2}$  where  $\mathbf{E}(\mathbf{b})$  represents the effective elasticity tensor of the mixture. Accordingly, the derivative expression (36) reduces to

$$\frac{d(\Delta \mathcal{F}_E)_{n+1}}{d\mathbf{b}} = \int_{\Omega_s} \Delta \boldsymbol{\varepsilon}_{n+1}^g : \left( \frac{\partial \sigma_{n+1/2}}{\partial \mathbf{b}} + \mathbf{E} : \mathbf{B} \cdot \frac{d\mathbf{u}_{n+1/2}}{d\mathbf{b}} \right) d\Omega_s \quad (37)$$

Direct differentiation of the state equation  $\mathbf{r}_{n+1/2} = \mathbf{0}$  (as opposed to the incremental state equation) provides

$$\frac{d\mathbf{u}_{n+1/2}}{d\mathbf{b}} = -\mathbf{K}^{-1} \cdot \int_{\Omega_s} \mathbf{B}^T : \frac{\partial \sigma_{n+1/2}}{\partial \mathbf{b}} d\Omega_s \quad (38)$$

Usage of this expression in (37) and simplifying yields

$$\frac{d(\Delta \mathcal{F}_E)_{n+1}}{d\mathbf{b}} = \int_{\Omega_s} (\Delta \boldsymbol{\varepsilon}_{n+1}^g + \boldsymbol{\varepsilon}_{n+1}^a) : \frac{\partial \sigma_{n+1/2}}{\partial \mathbf{b}} d\Omega_s \quad (39)$$

where  $\boldsymbol{\varepsilon}_{n+1}^a \equiv \sum_{A \in \{n-n_g\}} \mathbf{B}_A \cdot (\mathbf{u}_A^a)_{n+1}$  and where

$$(\mathbf{u}_A^a)_{n+1} \equiv -\mathbf{K}^{-1} \cdot \int_{\Omega_s} \mathbf{B}_A^T : \mathbf{E} : \Delta \boldsymbol{\varepsilon}_{n+1}^g d\Omega_s \quad (40)$$

plays the role of an adjoint displacement vector. For linear elastic structures, there is thus no need to explicitly compute or store either  $d\mathbf{u}/d\mathbf{b}$  or  $d\sigma/d\mathbf{b}$ .

3.3.2.2. *Special case 2: inviscid elastoplastic materials.* Two ways to implement generalized compliance design sensitivity analysis for structures comprised entirely of elastic-perfectly-plastic materials will be briefly discussed. For both methods, it is vital to note that the stress  $\sigma_{n+1/2}$  is path dependent and the stress update is of the form  $\Delta \sigma_{n+1} = \Delta \sigma_{n+1}(\mathbf{b}, \Delta \boldsymbol{\varepsilon}_{n+1})$ .

The first implementation is based on (36)<sub>1</sub> whereas the second is based on (36)<sub>2</sub>. For the first case, the full design gradient of the stress term in (36)<sub>1</sub> is written as

$$\frac{d\sigma_{n+1/2}}{d\mathbf{b}} = \frac{d\sigma_n}{d\mathbf{b}} + \frac{1}{2} \frac{\partial(\Delta \sigma_{n+1})}{\partial \mathbf{b}} + \frac{1}{2} \mathbf{C}_{n+1} : \mathbf{B} \cdot \frac{d(\Delta \mathbf{u}_{n+1})}{d\mathbf{b}} \quad (41)$$

where it is assumed that  $d\sigma_n/d\mathbf{b}$  has been stored and is available where required. Taking the full design gradient of the incremental state equation ( $\Delta \mathbf{r}_{n+1} = \mathbf{0}$ ) we obtain

$$\frac{d\Delta \mathbf{u}_{n+1}}{d\mathbf{b}} = -[\mathbf{K}_{n+1}]^{-1} \cdot \int_{\Omega_s} \mathbf{B}^T : \frac{\partial(\Delta \sigma_{n+1})}{\partial \mathbf{b}} d\Omega_s \quad (42)$$

Substitution of this expression into (36)<sub>1</sub> and simplifying yields

$$\frac{d(\Delta \mathcal{F}_E)_{n+1}}{d\mathbf{b}} = \int_{\Omega_s} \left[ \Delta \boldsymbol{\varepsilon}_{n+1}^g : \frac{d\sigma_n}{d\mathbf{b}} + \frac{1}{2} (\Delta \boldsymbol{\varepsilon}_{n+1}^g + \boldsymbol{\varepsilon}_{n+1}^a) : \frac{\partial(\Delta \sigma_{n+1})}{\partial \mathbf{b}} \right] d\Omega_s \quad (43)$$

where  $\boldsymbol{\varepsilon}_{n+1}^a = \mathbf{B} \cdot \mathbf{u}_{n+1}^a$  in which  $\mathbf{u}_{n+1}^a$  plays the role of an adjoint displacement vector obtained as

$$\mathbf{u}_{n+1}^a = -[\mathbf{K}_{n+1}]^{-1} \cdot \int_{\Omega_s} \mathbf{B}^T : \mathbf{C}_{n+1} : \Delta \boldsymbol{\varepsilon}_{n+1}^g d\Omega_s \quad (44)$$

Following the update of the strain energy increment by (43), the full design gradient of the stress ( $d\boldsymbol{\sigma}_{n+1}/d\mathbf{b}$ ) must be updated in those finite elements which have nodes on  $\Gamma_g$  (or those elements in which  $\Delta\boldsymbol{\varepsilon}^g$  does not vanish). The form of the stress design gradient update for usage in DSA during ensuing time steps is as follows:

$$\frac{d\boldsymbol{\sigma}_{n+1}}{d\mathbf{b}} = \frac{d\boldsymbol{\sigma}_n}{d\mathbf{b}} + \frac{\partial\Delta\boldsymbol{\sigma}_{n+1}}{\partial\mathbf{b}} + \mathbf{C}_{n+1} : \mathbf{B} \cdot \frac{d(\Delta\mathbf{u}_{n+1})}{d\mathbf{b}} \quad (45)$$

Alternatively, the second method, rather than computing  $d\boldsymbol{\sigma}/d\mathbf{b}$ , computes and stores  $\mathbf{f}^{\text{int}}/d\mathbf{b}$  at the essential boundary condition nodes. Utilizing (41) and (42) one can obtain at the  $E$ th node the full design gradient of the increment to  $i$ th component of the internal force vector as

$$\frac{d(\Delta f_{Ei}^{\text{int}})_{n+1}}{d\mathbf{b}} = \int_{\Omega_S} \mathbf{e}_i \cdot \mathbf{B}_E^T : \frac{\partial(\Delta\boldsymbol{\sigma}_{n+1})}{\partial\mathbf{b}} d\Omega_S + (\mathbf{u}_{Ei}^a)_{n+1}^T \cdot \int_{\Omega_S} \mathbf{B}^T : \frac{\partial(\Delta\boldsymbol{\sigma}_{n+1})}{\partial\mathbf{b}} d\Omega_S \quad (46)$$

where in this case,

$$(\mathbf{u}_{Ei}^a)_{n+1} = -[\mathbf{K}_{n+1}]^{-1} \cdot \int_{\Omega_S} \mathbf{B}^T : \mathbf{C}_{n+1} : \mathbf{B}_E \cdot \mathbf{e}_i d\Omega_S \quad (47)$$

plays the role of a dimensionless adjoint displacement vector  $\in \mathfrak{R}^{\text{neq}}$ , and  $\mathbf{e}_i$  is a unit vector in the  $i$ th coordinate direction. After updating the design gradient of the strain energy functional by (36)<sub>2</sub>, the design gradient of the internal force at essential boundary condition nodes are updated for usage in DSA at subsequent time steps.

*Remark 3.5.* When the structure is displacement-loaded at only a few nodes, the apparent advantage lies with the second approach in that it takes less memory to store the design gradient of the internal force vector at the applied non-vanishing displacement nodes  $E \in \{n_g\}$  than to store  $d\boldsymbol{\sigma}/d\mathbf{b}$  at the integration points in those elements having nodes on  $\Gamma_g$ .

#### 4. VOIGT AND REUSS MIXING RULE ALGORITHMS

##### 4.1. Overview of proposed framework

Many commercial and research finite element codes today have wide assortments of material model libraries including for example elasticity, elastoplasticity, viscoelasticity, viscoplasticity, continuum damage mechanics, endochronic models, and numerous others. The proposed Voigt and Reuss mixing rule integration algorithms developed below are potentially attractive in that they hold the possibility of enabling general purpose FEM codes to use their wide assortment of implemented material models in structural topology design optimization calculations. A modular framework is investigated below (Figure 2) in which existing material model numerical implementations are used with only minor modifications in topology optimization calculations.

Displacement-based finite element operations require stresses  $\boldsymbol{\sigma}$  and material tangent operators  $\mathbf{C} = \partial(\Delta)\boldsymbol{\sigma}/\partial(\Delta\boldsymbol{\varepsilon})$  as combined functions of such quantities as strains  $\boldsymbol{\varepsilon}$ ; strain increments  $\Delta\boldsymbol{\varepsilon}$ ; strain rates  $\dot{\boldsymbol{\varepsilon}}$ , and internal state variables  $\boldsymbol{\xi}$  which are history dependent. To facilitate the usage of a wide range of material models in structural analysis calculations, general purpose FEM analysis codes update stresses  $\boldsymbol{\sigma}$  and internal variables  $\boldsymbol{\xi}$  and compute material tangent operators

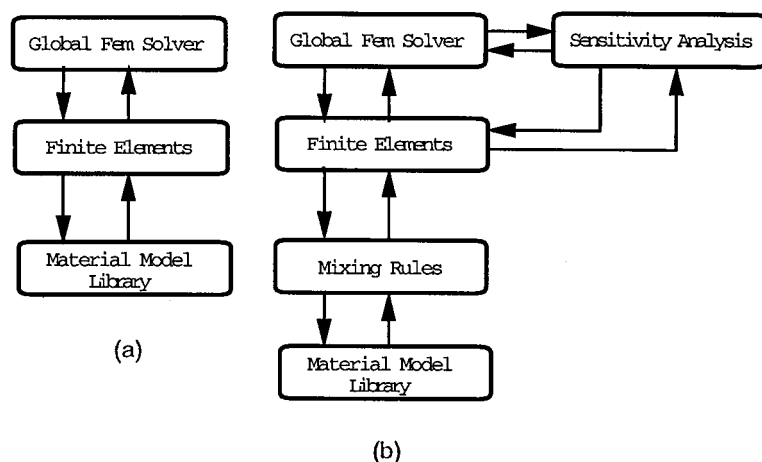


Figure 2. Investigated changes to architecture for implementation of topology optimization in general purpose FEM codes: (a) standard FEM architecture; (b) modified FEM architecture

**C** in modular material model libraries (Figure 2(a)). In the proposed continuous topology optimization framework, Voigt and Reuss mixing algorithms are employed as intermediaries between finite element routines and material model libraries. The Voigt and Reuss mixing routines algorithmically compute incremental constitutive behaviours for multi-material mixtures by enforcing the respective Voigt and Reuss assumptions. The incremental constitutive behaviours of the mixtures depend upon the volume fractions of the material phases present, the mixing rule assumption, and the characteristics of the phases being combined. With this very general approach, broad classes of materials can be treated, and only minor algorithmic changes are required to finite element operations and material model libraries. Naturally, it is assumed that working constitutive model implementations exist *a priori* for the materials whose topological layout is being designed on the global structural scale.

The problem of integrating rate constitutive models for individual inelastic solids has received extensive treatment in the literature in the past two decades, as for example in the case of small strains in Ref. 38–41. Here, our goal is to extend such works to the task of obtaining the integrated constitutive behaviour of mixtures of materials. The relatively standard problem of integrating general inelastic rate constitutive equations for a generic material phase  $\mathcal{A}$  within a displacement FEM framework can be stated as follows: On the time interval of interest  $[0, T] \subset \mathfrak{R}$ , it is assumed that at time  $t_n$  the strain  $\boldsymbol{\varepsilon}_n^{\mathcal{A}}$ , stress  $\boldsymbol{\sigma}_n^{\mathcal{A}}$  and internal state variables  $\boldsymbol{\xi}_n^{\mathcal{A}}$  at a fixed material point  $\mathbf{X}$  are known quantities; that is  $\{\boldsymbol{\varepsilon}_n^{\mathcal{A}}; \boldsymbol{\sigma}_n^{\mathcal{A}}; \boldsymbol{\xi}_n^{\mathcal{A}}\}$  are known at time  $t_n$ . The incremental displacement field  $\Delta \mathbf{u}_{n+1} : \Omega_S \rightarrow \mathfrak{R}^3$  over the time step  $[t_n, t_{n+1}]$  is assumed to be given. The problem of interest is thus to update the known quantities  $\{\boldsymbol{\varepsilon}_n^{\mathcal{A}}; \boldsymbol{\sigma}_n^{\mathcal{A}}; \boldsymbol{\xi}_n^{\mathcal{A}}\}$  from the end of the previous time step to their values  $\{\boldsymbol{\varepsilon}_{n+1}^{\mathcal{A}}; \boldsymbol{\sigma}_{n+1}^{\mathcal{A}}; \boldsymbol{\xi}_{n+1}^{\mathcal{A}}\}$  at  $t_{n+1}$  in a fashion consistent with appropriate rate constitutive equations. Within a displacement finite element formulation, the problem is generally treated as strain driven in that the total small strain tensor is exactly updated by the relation

$$\boldsymbol{\varepsilon}_{n+1}^{\mathcal{A}} = \boldsymbol{\varepsilon}_n^{\mathcal{A}} + \Delta \boldsymbol{\varepsilon}_{n+1}^{\mathcal{A}} = \boldsymbol{\varepsilon}_n^{\mathcal{A}} + \mathbf{B} \cdot (\Delta \mathbf{u})_{n+1} \quad (48)$$

The remaining dependent variables  $\{\sigma_{n+1}^{\mathcal{A}}; \xi_{n+1}^{\mathcal{A}}\}$  must be updated by integration of the rate equations for material phase  $\mathcal{A}$ . The stress increment over the time step for generic material phases is assumed to be of the form:  $\Delta\sigma_{n+1}^{\mathcal{A}} = \Delta\sigma_{n+1}^{\mathcal{A}}(\sigma_n^{\mathcal{A}}; \varepsilon_n^{\mathcal{A}}; \Delta\varepsilon_{n+1}^{\mathcal{A}})$ . In the following subsections, this generic constitutive update for a single material phase is generalized to the cases of two-phased Voigt mixtures (Section 4.2) and two-phased Reuss mixtures (Section 4.3).

#### 4.2. The Voigt mixing rule

Using numerical integration algorithms for individual inelastic materials, the Voigt mixing algorithm is naturally straightforward to implement in a displacement FEM setting. For all  $t \in [0, T]$  it is assumed that both material phases in a local mixture share the same history of strain,  $\varepsilon^{\mathcal{A}}(\mathbf{X}, t) = \varepsilon^{\mathcal{B}}(\mathbf{X}, t)$ . The algorithmic stress–strain characteristics of the mixture over a time interval  $[t_n, t_{n+1}]$  and the strain and design derivatives are presented below in Box 1.

##### Box 1. Voigt mixing rule algorithm

Given  $\{\sigma_n^{\mathcal{A}}, \xi_n^{\mathcal{A}}, \varepsilon_n^{\mathcal{A}}, \Delta\varepsilon_{n+1}\}$  compute  $\{\sigma_{n+1}^{\mathcal{A}}; \xi_{n+1}^{\mathcal{A}}; \varepsilon_{n+1}^{\mathcal{A}}; \frac{d\Delta\sigma^{\mathcal{A}}}{d\Delta\varepsilon}\}$

Given  $\{\sigma_n^{\mathcal{B}}, \xi_n^{\mathcal{B}}, \varepsilon_n^{\mathcal{B}}, \Delta\varepsilon_{n+1}\}$  compute  $\{\sigma_{n+1}^{\mathcal{B}}; \xi_{n+1}^{\mathcal{B}}; \varepsilon_{n+1}^{\mathcal{B}}; \frac{d\Delta\sigma^{\mathcal{B}}}{d\Delta\varepsilon}\}$

Assemble the mixture stress as weighted sum of partial stresses:

$$\sigma_{n+1} = \phi_{\mathcal{A}}\sigma_{n+1}^{\mathcal{A}} + \phi_{\mathcal{B}}\sigma_{n+1}^{\mathcal{B}} \quad (49)$$

Compute tangent operator of the mixture:

$$\mathbf{C}_{n+1} = \frac{d(\Delta\sigma)_{n+1}}{d(\Delta\varepsilon)_{n+1}} = \phi_{\mathcal{A}} \frac{d(\Delta\sigma^{\mathcal{A}})_{n+1}}{d(\Delta\varepsilon)_{n+1}} + \phi_{\mathcal{B}} \frac{d(\Delta\sigma^{\mathcal{B}})_{n+1}}{d(\Delta\varepsilon)_{n+1}} \quad (50a)$$

$$= \phi_{\mathcal{A}}\mathbf{C}_{n+1}^{\mathcal{A}} + \phi_{\mathcal{B}}\mathbf{C}_{n+1}^{\mathcal{B}} \quad (50b)$$

Compute the explicit design gradient of stress increment:

$$\frac{\partial\Delta\sigma_{n+1}}{\partial\phi_{\mathcal{A}}} = \Delta\sigma_{n+1}^{\mathcal{A}} - \Delta\sigma_{n+1}^{\mathcal{B}} \quad (51a)$$

$$\frac{\partial\Delta\sigma_{n+1}}{\partial\phi_{\mathcal{B}}} = \Delta\sigma_{n+1}^{\mathcal{B}} - \Delta\sigma_{n+1}^{\mathcal{A}} \quad (51b)$$

#### 4.3. Reuss mixing algorithm

**4.3.1. Integration algorithm.** For simplicity, implementation of the Reuss mixing rule is presented here for the special case of two materials that feature non-softening behaviours, in the sense of Drucker's definition.<sup>42</sup> The materials can be either isotropic, or anisotropic, but if they are anisotropic, their orientations are not considered to be designable in the present topology framework. Since nonlinear constitutive material behaviours are assumed (linear material behaviours are recovered as a trivial special case) the constitutive relations of both phases  $\mathcal{A}$  and  $\mathcal{B}$  at each integration point of the design domain  $\Omega_S$  are solved incrementally. Thus when global force

balance convergence is achieved in accordance with equation (17) at the  $n$ th time step of the global analysis problem, we have at each integration point of the structural domain  $\Omega_S$  a collection of equilibrium stresses, strains, and internal state variables associated with both material phases:  $(\boldsymbol{\sigma}_n^{\mathcal{A}}, \boldsymbol{\varepsilon}_n^{\mathcal{A}}, \zeta_n^{\mathcal{A}})$ ;  $(\boldsymbol{\sigma}_n^{\mathcal{B}}, \boldsymbol{\varepsilon}_n^{\mathcal{B}}, \zeta_n^{\mathcal{B}})$ . At a given integration point  $\mathbf{X}$  in the body, the global incremental displacement vector  $\Delta \mathbf{u}_{n+1}$  gives rise to a total strain increment as by equation (48). The objective of the Reuss mixing algorithm is to increment the stresses, strains and internal variables for the two material phases  $\mathcal{A}$  and  $\mathcal{B}$  so that the Reuss mixture constraints are satisfied:

$$\Delta \boldsymbol{\varepsilon}_{n+1} = \phi_{\mathcal{A}} \Delta \boldsymbol{\varepsilon}_{n+1}^{\mathcal{A}} + \phi_{\mathcal{B}} \Delta \boldsymbol{\varepsilon}_{n+1}^{\mathcal{B}} \quad (52a)$$

$$\mathbf{0} = \boldsymbol{\sigma}_{n+1}^{\mathcal{A}} - \boldsymbol{\sigma}_{n+1}^{\mathcal{B}} \quad (52b)$$

The first constraint (52a) simply requires that the volume fraction weighted strain increments in the respective material phases sum to the total strain increment, while the second constraint (52b) requires that both material phases at a fixed point satisfy the uniform stress requirement. In simple terms, the total strain increment  $\Delta \boldsymbol{\varepsilon}_{n+1}$  must be decomposed into individual strain increments  $\Delta \boldsymbol{\varepsilon}_{n+1}^{\mathcal{A}}$  and  $\Delta \boldsymbol{\varepsilon}_{n+1}^{\mathcal{B}}$  so as to satisfy the uniform stress requirement. For general constitutive material behaviours (other than linear elasticity) the satisfaction of these constraints is non-trivial and requires an iterative solution algorithm.

To begin defining this algorithm, a residual function  $\mathbf{r}^R$  for the uniform stress Reuss assumption is defined as

$$\mathbf{r}_{n+1}^R = \boldsymbol{\sigma}_{n+1}^{\mathcal{A}} - \boldsymbol{\sigma}_{n+1}^{\mathcal{B}} \quad (53)$$

and an index  $i$  is introduced to keep count of the iterations required to satisfy (52a) and (52b). Linearization of the residual function  $\mathbf{r}^R$  (53) allows for

$$\mathbf{r}_{n+1}^R \doteq \mathbf{r}_n^R + \frac{d\Delta \mathbf{r}_n^R}{d(\Delta \boldsymbol{\varepsilon})_n} : \Delta \boldsymbol{\varepsilon}_{n+1} \quad (54a)$$

$$= \mathbf{0} + \frac{d\Delta \mathbf{r}_n^R}{d(\Delta \boldsymbol{\varepsilon})_n} : \frac{d(\Delta \boldsymbol{\varepsilon}^{\mathcal{A}})_{n+1}}{d(\Delta \boldsymbol{\varepsilon})_{n+1}} : \Delta \boldsymbol{\varepsilon}_{n+1} + \frac{d\Delta \mathbf{r}_n^R}{d(\Delta \boldsymbol{\varepsilon})_n} : \frac{d(\Delta \boldsymbol{\varepsilon}^{\mathcal{B}})_{n+1}}{d(\Delta \boldsymbol{\varepsilon})_{n+1}} : \Delta \boldsymbol{\varepsilon}_{n+1} \quad (54b)$$

$$= \mathbf{C}_n^{\mathcal{A}} : \Delta \boldsymbol{\varepsilon}_{n+1}^{\mathcal{A}} - \mathbf{C}_n^{\mathcal{B}} : \Delta \boldsymbol{\varepsilon}_{n+1}^{\mathcal{B}} \quad (54c)$$

$$\doteq \mathbf{0} \quad (54d)$$

That  $\mathbf{r}_n^R = \mathbf{0}$  was assumed in (54b) follows from the assumption that the constraint (52b) was satisfied in the iterations at the  $n$ th time step. To obtain a good starting strain increment  $\Delta \boldsymbol{\varepsilon}_{n+1}$  decomposition among the material phases, incrementally elastic behaviour for both material phases is initially assumed in the  $(n+1)$ th step. Accordingly, equation (54) reduces to:

$$\mathbf{E}^{\mathcal{A}} : \Delta \boldsymbol{\varepsilon}_{n+1}^{\mathcal{A}} = \mathbf{E}^{\mathcal{B}} : \Delta \boldsymbol{\varepsilon}_{n+1}^{\mathcal{B}} \quad (55)$$

where  $\mathbf{E}^{\mathcal{A}}$  and  $\mathbf{E}^{\mathcal{B}}$  are incremental elastic constitutive tensor for materials  $\mathcal{A}$  and  $\mathcal{B}$ , respectively. Combining (52a) and (55) permits the partitioning of the total strain increment into two elastic strain increments that satisfy both (52a) and (52b):

$$\Delta \boldsymbol{\varepsilon}_{n+1}^{\mathcal{A},0} = [\phi_{\mathcal{B}} \mathbf{E}^{\mathcal{A}} + \phi_{\mathcal{A}} \mathbf{E}^{\mathcal{B}}]^{-1} : \mathbf{E}^{\mathcal{B}} : \Delta \boldsymbol{\varepsilon}_{n+1} \quad (56a)$$

$$\Delta \boldsymbol{\varepsilon}_{n+1}^{\mathcal{B},0} = [\phi_{\mathcal{B}} \mathbf{E}^{\mathcal{A}} + \phi_{\mathcal{A}} \mathbf{E}^{\mathcal{B}}]^{-1} : \mathbf{E}^{\mathcal{A}} : \Delta \boldsymbol{\varepsilon}_{n+1} \quad (56b)$$

The material strain increments  $\Delta\boldsymbol{\varepsilon}_{n+1}^{\mathcal{A},0}$  and  $\Delta\boldsymbol{\varepsilon}_{n+1}^{\mathcal{B},0}$  thus provide reasonable *first guesses* for the partitioned strain increments in materials  $\mathcal{A}$  and  $\mathcal{B}$ , respectively, based on the assumption of incremental elasticity. If either of the materials has an inelastic response over the strain increment, the uniform stress requirement (52b) will be violated. In this case, the Newton's Method procedure outlined in Box 2 is used to iteratively solve for the partitioning of the total strain increment  $\Delta\boldsymbol{\varepsilon}_{n+1}$  to satisfy (52a) and (52b) for inelastic materials. Upon obtaining convergence in Box 2, the final stress update is performed.

4.3.2. *Differentiation of the mixing rule.* Within the context of the combined analysis and design optimization problem, it is necessary to take both the strain and volume fraction derivatives of the proposed integration algorithm. The strain derivative gives the so-called 'consistent tangent operator', while the design derivative gives what will be called the 'stress design gradient'.

Box 2. Newton's method iterations for Reuss mixing rule

$i = 0$

Solve for initial strain sub-increments  $\Delta\boldsymbol{\varepsilon}_{n+1}^{\mathcal{A},0}$  and  $\Delta\boldsymbol{\varepsilon}_{n+1}^{\mathcal{B},0}$  by (56).

Compute:

$$\boldsymbol{\sigma}_{n+1}^{\mathcal{A},i} = \boldsymbol{\sigma}_{n+1}^{\mathcal{A},i}(\boldsymbol{\sigma}_n^{\mathcal{A}}, \boldsymbol{\varepsilon}_n^{\mathcal{A}}, \boldsymbol{\xi}_n^{\mathcal{A}}, \Delta\boldsymbol{\varepsilon}_{n+1}^{\mathcal{A},i}) \quad (57)$$

$$\boldsymbol{\sigma}_{n+1}^{\mathcal{B},i} = \boldsymbol{\sigma}_{n+1}^{\mathcal{B},i}(\boldsymbol{\sigma}_n^{\mathcal{B}}, \boldsymbol{\varepsilon}_n^{\mathcal{B}}, \boldsymbol{\xi}_n^{\mathcal{B}}, \Delta\boldsymbol{\varepsilon}_{n+1}^{\mathcal{B},i}) \quad (58)$$

$$\mathbf{r}_{n+1}^{\mathcal{R},i} = \boldsymbol{\sigma}_{n+1}^{\mathcal{A},i} - \boldsymbol{\sigma}_{n+1}^{\mathcal{B},i} \quad (59)$$

If  $\|\mathbf{r}_{n+1}^{\mathcal{R},i}\| \leq \text{TOL}$ , Then Converged Achieved, Exit.

Otherwise:

$$\Delta(\Delta\boldsymbol{\varepsilon}_{n+1}^{\mathcal{A},i}) = [\phi_{\mathcal{B}}\mathbf{C}^{\mathcal{A}} + \phi_{\mathcal{A}}\mathbf{C}^{\mathcal{B}}]^{-1} : -\phi_{\mathcal{B}}\mathbf{r}_{n+1}^{\mathcal{R},i} \quad (60)$$

$$\Delta(\Delta\boldsymbol{\varepsilon}_{n+1}^{\mathcal{B},i}) = [\phi_{\mathcal{B}}\mathbf{C}^{\mathcal{A}} + \phi_{\mathcal{A}}\mathbf{C}^{\mathcal{B}}]^{-1} : +\phi_{\mathcal{A}}\mathbf{r}_{n+1}^{\mathcal{R},i} \quad (61)$$

$$\Delta\boldsymbol{\varepsilon}_{n+1}^{\mathcal{A},i+1} = \Delta\boldsymbol{\varepsilon}_{n+1}^{\mathcal{A},i} + \Delta(\Delta\boldsymbol{\varepsilon}_{n+1}^{\mathcal{A},i}) \quad (62)$$

$$\Delta\boldsymbol{\varepsilon}_{n+1}^{\mathcal{B},i+1} = \Delta\boldsymbol{\varepsilon}_{n+1}^{\mathcal{B},i} + \Delta(\Delta\boldsymbol{\varepsilon}_{n+1}^{\mathcal{B},i}) \quad (63)$$

$$i = i + 1 \quad (64)$$

Return to (57)

4.3.3. *Consistent tangent operator.* Upon having solved for the partitioning of the fixed strain increment  $\Delta\boldsymbol{\varepsilon}_{n+1}$  that satisfies (52a) and (52b) for the  $(n+1)$ th time step through the algorithm in Box 2, the next task is to linearize the constraint (52b) about the converged state for a different strain increment which will be called  $\Delta\boldsymbol{\varepsilon}_{n+\beta}$ . Doing so at a typical integration point thus gives:

$$\mathbf{r}_{n+\beta}^{\mathcal{R}} \doteq \mathbf{r}_{n+1}^{\mathcal{R}} + \frac{\partial \mathbf{r}_{n+1}^{\mathcal{R}}}{\partial (\Delta\boldsymbol{\varepsilon}^{\mathcal{A}})_{n+1}} : \Delta\boldsymbol{\varepsilon}_{n+\beta}^{\mathcal{A}} + \frac{\partial \mathbf{r}_{n+1}^{\mathcal{R}}}{\partial (\Delta\boldsymbol{\varepsilon}^{\mathcal{B}})_{n+1}} : \Delta\boldsymbol{\varepsilon}_{n+\beta}^{\mathcal{B}} \quad (65a)$$

$$\doteq \mathbf{C}_{n+1}^{\mathcal{A}} : \Delta\boldsymbol{\varepsilon}_{n+\beta}^{\mathcal{A}} - \mathbf{C}_{n+1}^{\mathcal{B}} : \Delta\boldsymbol{\varepsilon}_{n+\beta}^{\mathcal{B}} \quad (65b)$$

$$\doteq \mathbf{0} \quad (65c)$$

Clearly, the new strain increment will also have to satisfy the partitioning constraint

$$\Delta \boldsymbol{\varepsilon}_{n+\beta} = \phi_{\mathcal{A}} \Delta \boldsymbol{\varepsilon}_{n+\beta}^{\mathcal{A}} + \phi_{\mathcal{B}} \Delta \boldsymbol{\varepsilon}_{n+\beta}^{\mathcal{B}} \tag{66}$$

Combining (65) and (66) thus provides linearized estimates of  $\Delta \boldsymbol{\varepsilon}_{n+\beta}^{\mathcal{A}}$  and  $\Delta \boldsymbol{\varepsilon}_{n+\beta}^{\mathcal{B}}$ :

$$\Delta \boldsymbol{\varepsilon}_{n+\beta}^{\mathcal{A}} = [\phi_{\mathcal{B}} \mathbf{C}_{n+1}^{\mathcal{A}} + \phi_{\mathcal{A}} \mathbf{C}_{n+1}^{\mathcal{B}}]^{-1} : \mathbf{C}_{n+1}^{\mathcal{B}} : \Delta \boldsymbol{\varepsilon}_{n+\beta} \tag{67a}$$

$$\Delta \boldsymbol{\varepsilon}_{n+\beta}^{\mathcal{B}} = [\phi_{\mathcal{B}} \mathbf{C}_{n+1}^{\mathcal{A}} + \phi_{\mathcal{A}} \mathbf{C}_{n+1}^{\mathcal{B}}]^{-1} : \mathbf{C}_{n+1}^{\mathcal{A}} : \Delta \boldsymbol{\varepsilon}_{n+\beta} \tag{67b}$$

The predicted stress increment consistent with linearization of the Reuss mixing algorithm stress update is, thus,

$$\Delta \boldsymbol{\sigma}_{n+\beta} = \mathbf{C}_{n+1}^{\mathcal{A}} : \Delta \boldsymbol{\varepsilon}_{n+\beta}^{\mathcal{A}} = \mathbf{C}_{n+1}^{\mathcal{B}} : \Delta \boldsymbol{\varepsilon}_{n+\beta}^{\mathcal{B}} \tag{68}$$

Differentiation of this expression with respect to  $\Delta \boldsymbol{\varepsilon}_{n+\beta}$ , employing (66), and setting  $\beta = 1$  thus gives the consistent tangent operator for the Reuss mixing rule algorithm:

$$\frac{d(\Delta \boldsymbol{\sigma}_{n+1})}{d(\Delta \boldsymbol{\varepsilon}_{n+1})} \doteq \mathbf{C}_{n+1}^{\mathcal{A}} : \frac{d(\Delta \boldsymbol{\varepsilon}_{n+1}^{\mathcal{A}})}{d(\Delta \boldsymbol{\varepsilon}_{n+1})} = \mathbf{C}_{n+1}^{\mathcal{B}} : \frac{d(\Delta \boldsymbol{\varepsilon}_{n+1}^{\mathcal{B}})}{d(\Delta \boldsymbol{\varepsilon}_{n+1})} \tag{69a}$$

$$= \mathbf{C}_{n+1}^{\mathcal{A}} : [\phi_{\mathcal{B}} \mathbf{C}_{n+1}^{\mathcal{A}} + \phi_{\mathcal{A}} \mathbf{C}_{n+1}^{\mathcal{B}}]^{-1} : \mathbf{C}_{n+1}^{\mathcal{B}} \tag{69b}$$

$$= [\phi_{\mathcal{A}} (\mathbf{C}_{n+1}^{\mathcal{A}})^{-1} + \phi_{\mathcal{B}} (\mathbf{C}_{n+1}^{\mathcal{B}})^{-1}]^{-1} \tag{69c}$$

Symmetry of this operator (69) is contingent upon symmetry of the consistent tangent operators  $\mathbf{C}_{n+1}^{\mathcal{A}}$  and  $\mathbf{C}_{n+1}^{\mathcal{B}}$  of both material phases.

*4.3.4. The stress design gradient.* In the design sensitivity calculations presented in Section 3.3 it is necessary to compute  $\partial \Delta \boldsymbol{\sigma} / \partial \mathbf{b}$  which in a given element at the generic  $(n + 1)$ th time step, corresponds to computing either  $\partial \Delta \boldsymbol{\sigma}_{n+1} / \partial \phi_{\mathcal{A}}$  if  $\phi_{\mathcal{A}}$  is taken to be the independent element design variable, or  $\partial \Delta \boldsymbol{\sigma}_{n+1} / \partial \phi_{\mathcal{B}}$  if  $\phi_{\mathcal{B}}$  is taken to be the independent element design variable. (In these calculations, the displacement and strain fields are held fixed.) In the following,  $\phi_{\mathcal{A}}$  is taken as the independent variable and the dependent variable is obtained simply as  $\phi_{\mathcal{B}} = 1 - \phi_{\mathcal{A}}$ .

It is assumed that the stress update algorithms for materials being treated at the  $(n + 1)$ th time step are of the general form

$$\Delta \boldsymbol{\sigma}_{n+1}^{\mathcal{A}} = \Delta \boldsymbol{\sigma}_{n+1}^{\mathcal{A}} (\boldsymbol{\sigma}_n^{\mathcal{A}}; \boldsymbol{\varepsilon}_n^{\mathcal{A}}; \Delta \boldsymbol{\varepsilon}_{n+1}^{\mathcal{A}}) \tag{70a}$$

$$\Delta \boldsymbol{\sigma}_{n+1}^{\mathcal{B}} = \Delta \boldsymbol{\sigma}_{n+1}^{\mathcal{B}} (\boldsymbol{\sigma}_n^{\mathcal{B}}; \boldsymbol{\varepsilon}_n^{\mathcal{B}}; \Delta \boldsymbol{\varepsilon}_{n+1}^{\mathcal{B}}) \tag{70b}$$

which encompasses elasticity, viscoelasticity; elasto-plasticity; visco-plasticity; and numerous other forms of material constitutive models. Dealing first with the partial design derivative of the stress for material phase  $\mathcal{A}$ , we have

$$\frac{\partial \Delta \boldsymbol{\sigma}_{n+1}^{\mathcal{A}}}{\partial \phi_{\mathcal{A}}} = \mathbf{Y}_{n+1}^{\mathcal{A}} \frac{\partial \boldsymbol{\sigma}_n^{\mathcal{A}}}{\partial \phi_{\mathcal{A}}} + \mathbf{Z}_{n+1}^{\mathcal{A}} \frac{\partial \boldsymbol{\varepsilon}_n^{\mathcal{A}}}{\partial \phi_{\mathcal{A}}} + \mathbf{C}_{n+1}^{\mathcal{A}} \frac{\partial \Delta \boldsymbol{\varepsilon}_{n+1}^{\mathcal{A}}}{\partial \phi_{\mathcal{A}}} \tag{71}$$

where

$$\mathbf{Y}_{n+1}^{\mathcal{A}} \equiv \frac{\partial \Delta \boldsymbol{\sigma}_{n+1}^{\mathcal{A}}}{\partial \boldsymbol{\sigma}_n^{\mathcal{A}}}, \quad \mathbf{Z}_{n+1}^{\mathcal{A}} \equiv \frac{\partial \Delta \boldsymbol{\sigma}_{n+1}^{\mathcal{A}}}{\partial \boldsymbol{\varepsilon}_n^{\mathcal{A}}} \quad \text{and} \quad \mathbf{C}_{n+1}^{\mathcal{A}} \equiv \frac{\partial \Delta \boldsymbol{\sigma}_{n+1}^{\mathcal{A}}}{\partial \Delta \boldsymbol{\varepsilon}_{n+1}^{\mathcal{A}}}$$

It should be noted that  $\mathbf{C}_{n+1}^{\mathcal{A}}$  is simply the consistent tangent operator from the integration algorithm for material  $\mathcal{A}$ , whereas  $\mathbf{Y}_{n+1}^{\mathcal{A}}$  and  $\mathbf{Z}_{n+1}^{\mathcal{A}}$  are new matrix operators which must be returned from the constitutive model routines. At the  $(n+1)$ th time step, following the stress update to obtain  $\boldsymbol{\sigma}_{n+1}^{\mathcal{A}}$ , the first two terms on the right-hand side of (71) can be calculated directly as

$$\mathbf{Q}_{n+1}^{\mathcal{A}} = \mathbf{Y}_{n+1}^{\mathcal{A}} \frac{\partial \boldsymbol{\sigma}_n^{\mathcal{A}}}{\partial \phi_{\mathcal{A}}} + \mathbf{Z}_{n+1}^{\mathcal{A}} \frac{\partial \boldsymbol{\varepsilon}_n^{\mathcal{A}}}{\partial \phi_{\mathcal{A}}} \quad (72)$$

which permits re-writing (71) in the abbreviated form

$$\frac{\partial \Delta \boldsymbol{\sigma}_{n+1}^{\mathcal{A}}}{\partial \phi_{\mathcal{A}}} = \mathbf{Q}_{n+1}^{\mathcal{A}} + \mathbf{C}_{n+1}^{\mathcal{A}} \frac{\partial \Delta \boldsymbol{\varepsilon}_{n+1}^{\mathcal{A}}}{\partial \phi_{\mathcal{A}}} \quad (73)$$

By analogy, for material phase  $\mathcal{B}$

$$\frac{\partial \Delta \boldsymbol{\sigma}_{n+1}^{\mathcal{B}}}{\partial \phi_{\mathcal{A}}} = \mathbf{Q}_{n+1}^{\mathcal{B}} + \mathbf{C}_{n+1}^{\mathcal{B}} \frac{\partial \Delta \boldsymbol{\varepsilon}_{n+1}^{\mathcal{B}}}{\partial \phi_{\mathcal{A}}} \quad (74)$$

where

$$\mathbf{Q}_{n+1}^{\mathcal{B}} = \frac{\partial \Delta \boldsymbol{\sigma}_{n+1}^{\mathcal{B}}}{\partial \boldsymbol{\sigma}_n^{\mathcal{B}}} \frac{\partial \boldsymbol{\sigma}_n^{\mathcal{B}}}{\partial \phi_{\mathcal{A}}} + \frac{\partial \Delta \boldsymbol{\sigma}_{n+1}^{\mathcal{B}}}{\partial \boldsymbol{\varepsilon}_n^{\mathcal{B}}} \frac{\partial \boldsymbol{\varepsilon}_n^{\mathcal{B}}}{\partial \phi_{\mathcal{A}}} \quad (75)$$

In the computation of  $\mathbf{Q}_{n+1}^{\mathcal{A}}$  and  $\mathbf{Q}_{n+1}^{\mathcal{B}}$  it is assumed that  $\partial \boldsymbol{\sigma}_n / \partial \phi_{\mathcal{A}}$ ,  $\partial \boldsymbol{\varepsilon}_n^{\mathcal{A}} / \partial \phi_{\mathcal{A}}$  and  $\partial \boldsymbol{\varepsilon}_n^{\mathcal{B}} / \partial \phi_{\mathcal{A}}$  were computed and stored at the  $n$ th time step and are thus available in the operations of (72) and (75).

The remaining task is now to compute  $\partial \Delta \boldsymbol{\varepsilon}_{n+1}^{\mathcal{A}} / \partial \phi_{\mathcal{A}}$  and  $\partial \Delta \boldsymbol{\varepsilon}_{n+1}^{\mathcal{B}} / \partial \phi_{\mathcal{A}}$ . This is accomplished by taking the partial derivatives of the incremental strain decomposition equation (52a) and the uniform stress condition (52b) to obtain

$$\frac{\partial \Delta \boldsymbol{\varepsilon}_{n+1}^{\mathcal{A}}}{\partial \phi_{\mathcal{A}}} = [\phi_{\mathcal{B}} \mathbf{C}_{n+1}^{\mathcal{A}} + \phi_{\mathcal{A}} \mathbf{C}_{n+1}^{\mathcal{B}}]^{-1} [\phi_{\mathcal{B}} (\mathbf{Q}_{n+1}^{\mathcal{B}} - \mathbf{Q}_{n+1}^{\mathcal{A}}) + \mathbf{C}_{n+1}^{\mathcal{B}} (\Delta \boldsymbol{\varepsilon}_{n+1}^{\mathcal{B}} - \Delta \boldsymbol{\varepsilon}_{n+1}^{\mathcal{A}})] \quad (76a)$$

$$\frac{\partial \Delta \boldsymbol{\varepsilon}_{n+1}^{\mathcal{B}}}{\partial \phi_{\mathcal{A}}} = [\phi_{\mathcal{B}} \mathbf{C}_{n+1}^{\mathcal{A}} + \phi_{\mathcal{A}} \mathbf{C}_{n+1}^{\mathcal{B}}]^{-1} [\phi_{\mathcal{A}} (\mathbf{Q}_{n+1}^{\mathcal{A}} - \mathbf{Q}_{n+1}^{\mathcal{B}}) + \mathbf{C}_{n+1}^{\mathcal{A}} (\Delta \boldsymbol{\varepsilon}_{n+1}^{\mathcal{A}} - \Delta \boldsymbol{\varepsilon}_{n+1}^{\mathcal{B}})] \quad (76b)$$

The stress design gradient for the local mixture can then be calculated by either (73) or (74).

Since at the generic  $(n+1)$ th time step the stress derivative for the Reuss algorithm utilizes  $\partial \boldsymbol{\varepsilon}_n^{\mathcal{A}} / \partial \phi_{\mathcal{A}}$ ,  $\partial \boldsymbol{\varepsilon}_n^{\mathcal{B}} / \partial \phi_{\mathcal{A}}$  and  $\partial \boldsymbol{\sigma}_n / \partial \phi_{\mathcal{A}}$ , these quantities must be incremented and stored each time step. For example, at the  $(n+1)$ th time step one must update the strain partial derivatives for both phases by the relations:

$$\frac{\partial \boldsymbol{\varepsilon}_{n+1}^{\mathcal{A}}}{\partial \phi_{\mathcal{A}}} = \frac{\partial \boldsymbol{\varepsilon}_n^{\mathcal{A}}}{\partial \phi_{\mathcal{A}}} + \frac{\partial \Delta \boldsymbol{\varepsilon}_{n+1}^{\mathcal{A}}}{\partial \phi_{\mathcal{A}}} \quad (77a)$$

$$\frac{\partial \boldsymbol{\varepsilon}_{n+1}^{\mathcal{B}}}{\partial \phi_{\mathcal{A}}} = \frac{\partial \boldsymbol{\varepsilon}_n^{\mathcal{B}}}{\partial \phi_{\mathcal{A}}} + \frac{\partial \Delta \boldsymbol{\varepsilon}_{n+1}^{\mathcal{B}}}{\partial \phi_{\mathcal{A}}} \quad (77b)$$

These quantities are then stored at all integration points in the mesh of  $\Omega_S$  for usage in sensitivity analysis at subsequent time steps.

#### 4.4. Hybrid Voigt–Reuss mixtures

For certain classes of material behaviours, specifically elastic, perfectly-plastic behaviours, the pure Reuss mixing can feature a stress discontinuity at  $\phi_A = 1.0$  if phase  $\mathcal{A}$  is taken to be the stronger of the two materials. For this class of materials, and perhaps others, it is better to use hybrid Voigt–Reuss mixtures to avoid stress discontinuities in mixture behaviours. One simple way to hybridize the Voigt and Reuss mixing rules is to treat the local mixtures as having a volumetric fraction  $\alpha$  that behaves in accordance with the Voigt mixing rule and a volumetric fraction  $1 - \alpha$  that behaves in accordance with the Reuss mixing rule. The assumption is that both partitions of the hybrid mixture would have the same strain. Accordingly, the effective stresses and strains of the hybridized Voigt–Reuss mixture are

$$\boldsymbol{\varepsilon} = \boldsymbol{\varepsilon}_{\text{Voigt}} = \boldsymbol{\varepsilon}_{\text{Reuss}} \quad (77)$$

$$\boldsymbol{\sigma} = \alpha \boldsymbol{\sigma}_{\text{Voigt}} + (1 - \alpha) \boldsymbol{\sigma}_{\text{Reuss}} \quad (78)$$

There are numerous options on how one can treat the partitioning fraction  $\alpha$ . Here, it is proposed that  $\alpha$  be treated as follows:

$$\alpha = \left\{ \begin{array}{ll} \alpha_0 & 0 \leq \phi_{\mathcal{A}} \leq \phi_{\text{break}} \\ \alpha_0 + (1 - \alpha_0) \frac{(\phi_{\mathcal{A}} - \phi_{\text{break}})}{(1 - \phi_{\text{break}})} & \phi_{\text{break}} < \phi_{\mathcal{A}} \leq 1 \end{array} \right\} \quad (79)$$

where  $\alpha_0 \in [0, 1]$  and  $\phi_{\text{break}} \in (0, 1)$  are specified parameters that permit the designer/analyst to control the behaviour of the mixture.

## 5. SENSITIVITY ANALYSIS RESULTS

The intent of this section is to verify the consistency between the proposed design sensitivity algorithms presented in Section 3.3 and the structural analysis algorithms presented in Section 3.2 combined with the mixing rule algorithms presented in Section 4. This is accomplished by performing incremental structural analysis computations on a simple structural domains  $\Omega_S$  separately involving: linear elastic materials; elastoplastic materials; and viscoelastic materials. The design gradients of non-linear energy-type functionals are then computed using the sensitivity analysis algorithms presented in Section 3.3 and compared against very accurate design gradients computed by finite difference methods.

### 5.1. Material models employed

Due to the well-posedness of displacement–loaded structural problems, the design sensitivity algorithms of Section 3.3 are here verified on a number of inelastic displacement–loaded continuum structural problems. For simplicity, the material models employed in the following design sensitivity calculations are confined to: linear isotropic elasticity; elastoplasticity coupling linear isotropic elasticity with a simple von Mises yield criterion; and standard linear solid viscoelasticity. For the linear elastic materials, the Lamé moduli used for materials  $\mathcal{A}$  and  $\mathcal{B}$  are, respectively,  $\lambda_{\mathcal{A}} = 1.263E11$ ,  $\mu_{\mathcal{A}} = 1.18E11$  and  $\lambda_{\mathcal{B}} = 1.263E5$ ,  $\mu_{\mathcal{B}} = 1.18E5$ . For the elastoplastic design sensitivity tests, the material moduli for the solids are as listed above, while the respective von Mises yield strengths are  $Y_{\mathcal{A}} = 1.0E9$  and  $Y_{\mathcal{B}} = 1.0E3$ . For the viscoelastic DSA computations, the rate

Table I. Material parameters used in viscoelastic DSA tests

Parameter	Phase $\mathcal{A}$	Phase $\mathcal{B}$
$k_1$	1.238E10	2.000E08
$k_2$	1.238E07	2.000E05
$k_3$	1.000E04	1.000E02
$\mu_1$	1.130E10	1.200E08
$\mu_2$	1.130E06	1.200E05
$\mu_3$	1.000E04	1.000E02

form of constitutive equations employed are:

$$[\mathbf{E}_1 + \mathbf{E}_2] : \dot{\boldsymbol{\varepsilon}} + \mathbf{E}_1 : \boldsymbol{\eta}^{-1} : \mathbf{E}_2 \boldsymbol{\varepsilon} = \dot{\boldsymbol{\sigma}} + \mathbf{E}_1 : \boldsymbol{\eta}^{-1} : \boldsymbol{\sigma} \quad (80)$$

where  $\mathbf{E}_1$  and  $\mathbf{E}_2$  are linear isotropic elasticity tensors and  $\boldsymbol{\eta}$  is a linear isotropic viscosity tensor:

$$\mathbf{E}_1 = k_1 \mathbf{1} \otimes \mathbf{1} + \mu_1 \mathbf{I}_{\text{dev}} \quad (81a)$$

$$\mathbf{E}_2 = k_2 \mathbf{1} \otimes \mathbf{1} + \mu_2 \mathbf{I}_{\text{dev}} \quad (81b)$$

$$\boldsymbol{\eta} = k_3 \mathbf{1} \otimes \mathbf{1} + \mu_3 \mathbf{I}_{\text{dev}} \quad (81c)$$

in which  $k_1$  and  $k_2$  are bulk moduli,  $\mu_1$  and  $\mu_2$  are shear moduli, while  $k_3$  is a bulk viscosity and  $\mu_3$  a shear viscosity. For the viscoelastic design sensitivity analysis computations that follow, the material parameters for phases  $\mathcal{A}$  and  $\mathcal{B}$  are listed in Table I. The non-linear, or inelastic material models employed were implemented with backward Euler integration algorithms and consistent tangent operators for usage in design sensitivity analysis.

## 5.2. Sensitivity analysis results

For the sensitivity analysis tests to be performed, the structural domain  $\Omega_S$ , its mesh resolution, and the applied displacement loading are shown below in Figure 3. For simplicity, the domain is discretized into only four elements, and a symmetrical displacement loading is applied. Design gradients of the strain energy compliance functional defined by equation (19) are computed in elements 2 and 4 of  $\Omega_S$ . The design gradients are computed alternately using the DSA algorithms of Section 3, and by accurate finite difference calculations using the **DESIGN** optimization program<sup>43</sup>. The results are presented below in Table II. Due to the high accuracy of finite difference design gradients presented, the small differences between the DSA algorithm gradients and the finite difference gradients are attributed to approximations in the DSA algorithms associated with consistent linearization of non-linear problems. For the results presented below, each element of the structural domain contains a two-phased mixture of materials  $\mathcal{A}$  and  $\mathcal{B}$  ( $\phi_{\mathcal{A}} = \phi_{\mathcal{B}} = 0.50$ ). The structure is displacement-loaded separately for the cases where the materials are: linear elastic; elastoplastic; and viscoelastic. For each of the three material types considered, the mixture is first treated using the Voigt assumption and second using either the Reuss assumption or the hybrid Voigt–Reuss assumption.

The design sensitivity results of Table II show that for the class of problems treated here, the design gradient expressions presented in Section 3 agree with the nearly exact design gradients

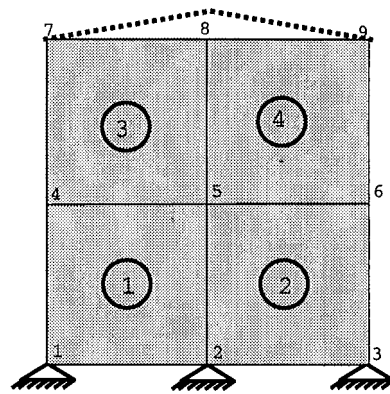


Figure 3. Coarse FEM mesh used to verify incremental DSA algorithms. The mesh is loaded by applying a vertical displacement at node #8

Table II. Compliance design gradients for displacement-loaded structure

Description*	DSA algorithm		Finite difference	
	Element #2	Element #4	Element #2	Element #4
	Linear elastic materials			
Voigt	-1.0280E9	-1.9904E9	-1.0279E9	-1.9903E9
Reuss	-4.1120E3	-7.9615E3	-4.1121E3	-7.9621E3
	Elasto-plastic materials			
Voigt	-5.8105E8	-1.3441E9	-5.8752E8	-1.3376E9
Voigt-Reuss†	-5.9695E4	-1.3750E5	-5.9600E4	-1.3525E5
	Visco-elastic materials			
Voigt	-5.2883E8	-1.0470E9	-5.2861E8	-1.0472E9
Reuss	-2.1187E7	-4.1753E7	-2.1119E7	-4.1824E7

\*Each test was performed in ten equal-displacement load steps

a. The linear elastic and elastoplastic tests were performed by applying a displacement of 0.25 over ten load steps

b. The viscoelastic tests were performed by applying a displacement of 2.5 over a time interval [0,2.5E-5]

†  $\alpha_0 = 0.0001$ ,  $\phi_{\text{break}} = 0.95$

computed by finite difference methods to within 2 per cent. For realistic topology design optimization problems involving a large number of design variables, computation of design gradients by finite difference methods is prohibitively expensive. Hence, the DSA methods verified here represent an efficient means of obtaining design gradient information of reasonably high accuracy. The agreement between the 'exact' and computed design gradients in Table II also demonstrates the consistency between the structural analysis techniques, wherein mixtures of general materials reside throughout the structural domain and are treated using the Voigt and Reuss incremental mixing algorithms, and the proposed design sensitivity techniques.

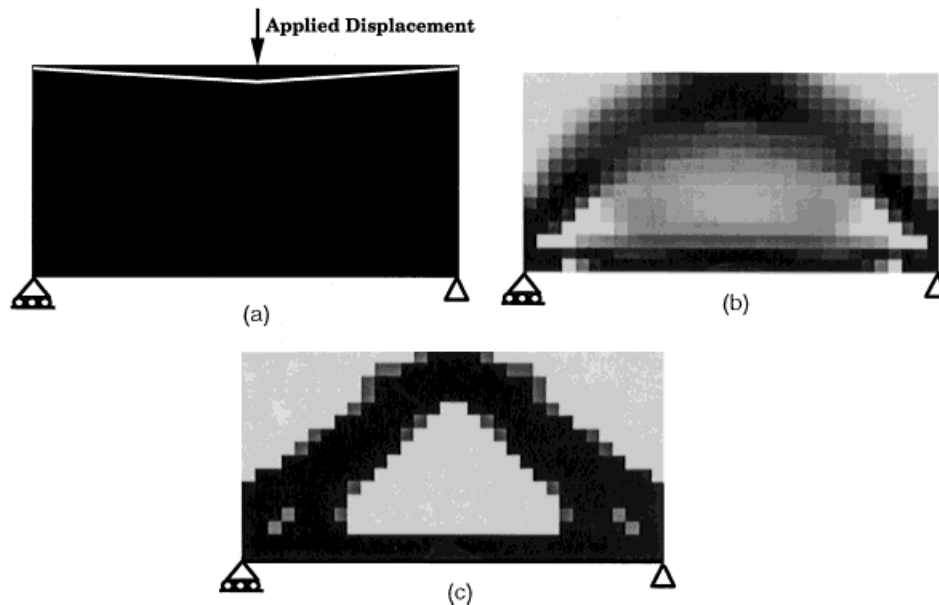


Figure 4. (a) Displacement-controlled strength optimization problem, with initial design state  $b_0 = 1.0$ ; (b) Solution obtained with a pure Voigt formulation ( $\Pi = -7.70E2$ ); and (c) Solution obtained with a hybrid Voigt-Reuss formulation ( $\Pi = -7.69E2$ )

### 5.3. Strength optimization of a Von Mises elastoplastic structure

While topology optimization has been widely used to design structures for high stiffnesses, the basic techniques have not been widely applied to strength optimization of continuum structures. With extended topology optimization frameworks of the type developed herein, such important classes of problems can begin to be explored. To demonstrate, the proposed framework is tested on an inelastic application involving the strength optimization of a relatively simple structure. A simply supported structural domain  $\Omega_S$  is subjected to monotonically applied, small vertical displacement loading applied as shown in Figure 4(a). At the peak displacement loading which is achieved in twenty load/time steps, ( $\delta/L = 5 \times 10^{-4}$ , where  $L$  is the span of the structure between supports), the structure has reached the limit of its resistive capacity. That is, further displacement load increments do not create further incremental resistance on the part of the structure. This two-material problem involves finding the optimal placement of an elastoplastic solid phase and a void phase. The solid phase, which is isotropic with elastic moduli  $\lambda_{\text{solid}} = 1.263 \times 10^{11}$ ,  $\mu_{\text{solid}} = 1.18 \times 10^{11}$  and a von Mises yield strength  $Y_{\text{solid}} = 10^6$ , initially fills the design domain  $\Omega_S$ . The void phase is treated as a highly compliant, linearly elastic solid with  $\lambda_{\text{void}} = 10^{-6} \lambda_{\text{solid}}$ ,  $\mu_{\text{void}} = 10^{-6} \mu_{\text{solid}}$ . The structural domain  $\Omega_S$  is discretized into 512 bilinear continuum finite elements. To avoid mesh-locking associated with isochoric elastoplastic deformation the B-bar formulation of Hughes is employed.<sup>44</sup> These computations were performed with the mesh filtering methods described in Reference 18 to avoid potential problems with checkerboarding solutions.

The topology design optimization problem is performed to maximize the strain energy  $\Pi$  in the structure [equation (12)] under the applied displacement loading, subject to a 50 per cent global

volume fraction constraint on the solid phase. Formally, the optimization problem is

$$\min_{\mathbf{b}} -\Pi(\mathbf{b}, \mathbf{u}(\mathbf{b})) = - \int_0^T \int_{\Gamma_g} \mathbf{n} \cdot \boldsymbol{\sigma} \cdot \dot{\mathbf{g}}(\tau) d\Gamma_g d\tau \quad \text{subject to} \quad (82a)$$

$$\mathcal{H} = \langle \phi_{\text{solid}} \rangle - 0.50 \leq 0 \quad (82b)$$

and

$$\mathbf{r}(\mathbf{b}, \mathbf{u}(\mathbf{b})) = \mathbf{0} \quad \text{on } \Omega_s \quad (82c)$$

This problem was solved using an SQP optimization algorithm with line searching<sup>43</sup>. The termination criteria were feasibility and satisfaction of the first-order optimality condition:

$$\left\| -\frac{d\Pi}{d\mathbf{b}} + v \frac{d\mathcal{H}}{d\mathbf{b}} \right\| \leq \text{TOL} \quad (83)$$

where  $v$  is the Lagrange multiplier associated the volume fraction constraint and TOL is a convergence parameter.

Two test computations were performed. In the first, which used the pure Voigt formulation ( $\alpha = 1$ ), the design achieved is that shown in Figure 4(b). Since Voigt mixtures are very stiff and strong, the optimal solution, obtained in 24 iterations, features a layout design making extensive usage of mixtures. To achieve a sharp, nearly discrete, and interpretable solution to this problem, it was solved a second time using a penalized hybrid Voigt–Reuss formulation ( $\alpha_0 = 0.001$ ;  $\phi_{\text{break}} = 0.95$ ). The resulting topology design is interpretable and nearly discrete (Figure 4(c)) and was obtained in 34 design optimization iterations.

#### 5.4. Strength optimization of Drucker–Prager elastoplastic structure

In many cases, the topology optimization of a structure for high stiffness in the elastic range of behaviour also optimizes the ultimate strength of the structure in the regime of inelastic material behaviour. There are also many cases, however, where designs optimized for minimal elastic compliance will differ substantially from those optimized for strength. For example, many construction materials such as concrete and masonry have similar stiffnesses in tension and compression, but show much greater strength in compression than in tension. One classical way to model such asymmetrical strength characteristics is with Mohr–Coulomb and/or Drucker–Prager-type elastoplastic material models. In the simple example below, a displacement load ( $\delta/L = 5.0 \times 10^{-5}$ ) is applied to a structure in twenty load steps. The structure is to be designed with a tension-weak/compression-strong material. The optimization problem is to design an optimal structure that can support the applied load in tension, compression, or some combination of both (Figure 5(a)). To show the difference between the linear elastic solutions and the elastoplastic solutions, the problem is solved first as a structural stiffness optimization problem, and secondly as a strength (or generalized stiffness) optimization problem. To assure the necessary smoothness and continuous differentiability of the material models, a Drucker–Prager elastoplasticity model with a circular tension cap and implemented with a fully implicit integration algorithm was employed to model the solid material (Figure 5(b)). The basic formulation of the problem is virtually identical to that of the preceding example with the exception that the structural domain, boundary conditions, and material behaviours are different. These topology design computations were performed without any methods to control possible checkerboarding solutions.

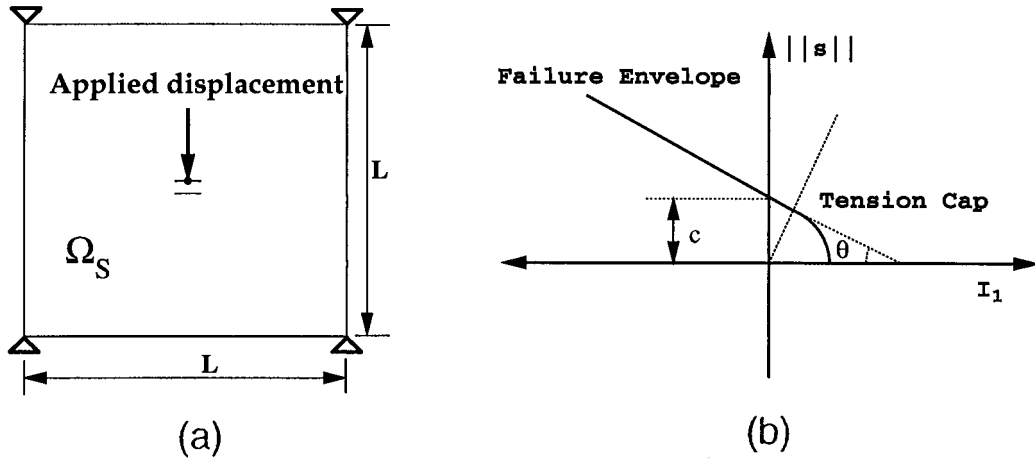


Figure 5. (a) Restraint and loading conditions on a fully designable structural domain  $\Omega_S$  to which an applied downward displacement is applied as shown; (b) Drucker–Prager elastoplasticity model which features strong compression and weak tension behaviours. In the model,  $\mathbf{S}$  denotes the deviatoric stress tensor, and  $I_1$  the trace of the stress tensor. Material values used in the computation are:  $\lambda = 1.26eE11$ ,  $\mu = 1.18E11$ ,  $c = 1.0E6$ ,  $\theta = 14^\circ$

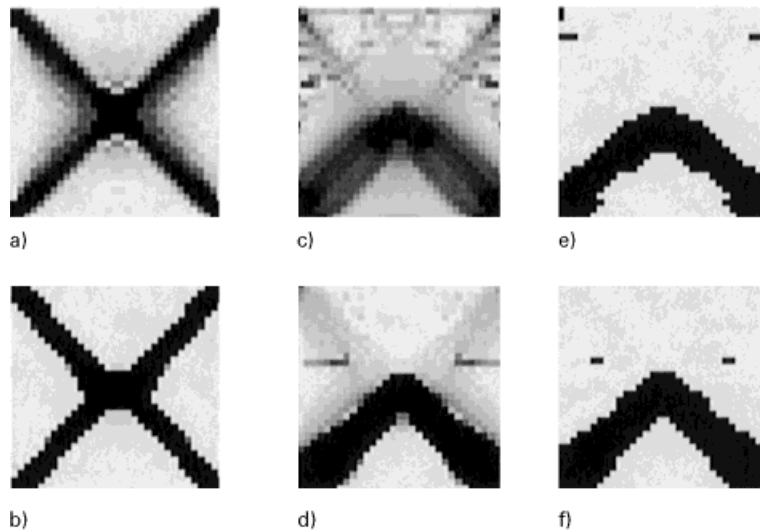


Figure 6. (a) Voigt elastic compliance minimization problem ( $\Pi = 9.07E1$ ); (b) Hybrid ( $\alpha = 0.05$ ) elastic compliance minimization problem ( $\Pi = 8.70E1$ ); (c) Voigt elastoplastic compliance minimization problem ( $\Pi = 7.70E3$ ); (d) Hybrid ( $\alpha = 0.05$ ,  $\phi_{\text{break}} = 0.95$ ) elastoplastic compliance minimization problem ( $\Pi = 6.90E3$ ); (e) Penalized Voigt elastoplastic compliance minimization problem ( $\Pi = 6.53E3$ ); (f) Hybrid ( $\alpha = 0.05$ ,  $\phi_{\text{break}} = 0.95$ ) elastoplastic compliance minimization problem ( $\Pi = 6.95E3$ )

The Voigt and hybrid Voigt–Reuss solutions to the elastic compliance minimization problem are shown in Figure 6(a) and 6(b). Since in the elastic regime of behaviour the material features symmetrical tension and compression behaviours, the elastic solution allows the structure to support

the applied displacement load in *both* tension and compression. When the applied load is made large enough to take the structure to its limit capacity, however, the optimal structure supports the load primarily in compression, since the material is stronger in compression. Thus an arch structure, as opposed to a suspension structure, is constructed on the bottom half of the structural domain. The Voigt solution is shown in Figure 6(c) and the hybrid Voigt–Reuss solution in Figure 6(d). Both solutions feature significant regions of grey left in the optimal design. To obtain a discrete final design, the optimization processes are continued with the introduction of an explicit constraint to eliminate intermediate volume fractions:  $\langle \phi_{\text{solid}}(1 - \phi_{\text{solid}}) \rangle \leq 0.01$ . The final designs are shown in Figures 6(e) and 6(f). Clearly for the material system employed, there is a significant difference between carrying the applied load in tension and compression. Since the proposed topology formulation can take detailed account of material constitutive behaviours, it rightly designs the optimal structure as a compression arch.

## 6. SUMMARY

A new formulation of the continuous structural topology optimization problem has been proposed and developed in this paper, complete with incremental design sensitivity analysis algorithms for non-linear applications. The novel formulation differs from many other relaxed topology formulations which utilize microstructured composites or mixtures of material phases, and instead uses amorphous mixtures whose constitutive properties are governed by the classical Voigt uniform strain and Reuss uniform stress assumptions, and hybrid combinations of the two. The utility of this alternative topology optimization framework is that it is very general and is directly applicable to topology design applications involving multiple general elastic and inelastic materials with very little effort required when new materials are employed in topology optimization, once the general framework (Figure 2(b)) is established.

In Reference 18 the new topology formulation was implemented and tested on linear elastic structural topology optimization problems involving solid phases and void phases. The characteristics of the Voigt, Reuss and hybrid formulations were studied with respect to uniqueness of designs, stability, discreteness, and interpretability. Here, the basic Voigt–Reuss topology optimization framework has been extended to the class of problems involving the layout of two general, elastic or inelastic non-softening solids within the confines of materially nonlinear, but geometrically linear structural analysis problems. Within this class of problems, the consistency between the structural analysis formulation, the Voigt and Reuss mixing algorithms, and the design sensitivity analysis methods have been verified for linear elastic materials, elastoplastic materials, and viscoelastic materials. Further work is now required to extend the framework to incorporate the treatment of inelastic material mixtures undergoing large strains and rotations.

Beyond the example topology problems solved here, the proposed methods have also been used with some considerable success in the material layout design of high-strength composites.<sup>13</sup> With extended topology design methods of the type developed herein, it is believed that a broad range of new problems can begin to be productively addressed with topology optimization methods, including: strength optimization of structural systems; design of structural systems for both stiffness and mechanical damping; and numerous others.

Finally, while the framework studied here has been developed using the classical Voigt and Reuss mixing rules, there are several alternative frameworks which can also treat mixtures of general inelastic materials as well. Most prominent would be topology optimization frameworks

based on power-law mixing rules, which can be straightforwardly implemented in much the same manner as the Voigt formulation and readily used with a wide class of inelastic materials. It is also worth noting that by introducing several simplifications into the homogenization based topology optimization framework of Bendsoe and Kikuchi<sup>1</sup>, Mayer *et al.*<sup>45</sup> have employed topology optimization to solve solid-void layout problems in crash-loaded structural elements involving a Prandtl–Reuss elastic–plastic material model. Since other frameworks can also treat inelastic materials, a question that warrants further study is which framework will ultimately prove to be most robust, computationally efficient, and versatile with a wide range of inelastic material models. In this regard, a potential strength of the Voigt–Reuss formulation deriving from its algorithmic nature is that it can be straightforwardly extended to solve optimal layout problems involving more than two materials. For example, in the concept design of frame structures for high stiffness and high mechanical damping, one might wish to employ topology design to solve for the optimal placement of a solid linear elastic phase, a viscoelastic damping phase, and a void phase. Furthermore, in the design of composite materials, one might wish to employ topology design to optimize the microstructural arrangement of  $N > 2$  material phases, which could feature either elastic or response behaviours. The Voigt–Reuss formulation is potentially attractive for such extended classes of topology design optimization problems.

## ACKNOWLEDGEMENTS

The authors acknowledge helpful and stimulating discussions on the very interesting subject of nonlinear design sensitivity analysis with Professor Jasbir S. Arora.

## REFERENCES

1. M. P. Bendsoe and N. Kikuchi, 'Generating optimal topology in structural design using a homogenization method', *Comput. Meth. Appl. Mech. Engng.*, **71**, 197–224 (1988).
2. C. S. Jog, R. B. Haber and M. P. Bendsoe, 'Topology design with optimized, self-adaptive materials', *Int. J. Numer. Meth. Engng.*, **37**, 1323–1350 (1994).
3. E. Hinton and J. Siensz, 'Aspects of adaptive finite element analysis and structural optimization', in B. H. V. Topping and M. Papadrakakis (eds), *Advances in Structural Optimization*, Civil-Comp Press, Edinburgh, 1994, pp. 1–25.
4. E. Ramm, K. -U. Bletzinger, R. Reitingner and K. Maute, 'The challenge of structural optimization', in B. H. V. Topping and M. Papadrakakis (eds), *Advances in Structural Optimization*, Civil-Comp Press, Edinburgh, 1994, pp. 27–53.
5. H. P. Mlejnek and R. Schirmacher, 'An engineer's approach to optimal material distribution and shape finding', *Comput. Meth. Appl. Mech. Engng.*, **106**, 1–26 (1993).
6. N. Kikuchi and K. Suzuki, 'Structural optimization of a linearly elastic structure using the homogenization method', in *Composite Media and Homogenization Theory*, Springer, Berlin, 1991, pp. 183–203.
7. M. P. Bendsoe, A. R. Diaz, R. Lipton and J. E. Taylor, 'Optimal design of material properties and material distribution for multiple loading conditions', *Int. J. Numer. Meth. Engng.*, **38**, 1149–1170 (1995).
8. G. Allaire and R. V. Kohn, 'Topology optimal design and optimal shape design using homogenization', in M. P. Bendsoe and C. A. Mota Soares (eds), *Topology Design of Structures*, Kluwer Academic Publishers, Dordrecht/Boston, 1993, pp. 207–218.
9. A. R. Diaz and M. P. Bendsoe, 'Shape optimization of structures for multiple loading conditions using a homogenization method', *Struct. Optim.*, **4**, 17–22 (1992).
10. H. C. Gea, 'Topology optimization: a new micro-structure based design domain method', *ASME Des. Engng. Div. DE*, **69-2**, 283–290 (1994).
11. O. Sigmund, 'Design of material structures using topology optimization', *Report S69*, Danish Center for Applied Mathematics and Mechanics, December 1994.
12. C. C. Swan and I. Kosaka, 'Homogenization-based analysis and design of composites', *Comput. and Struct.*, **63**, (124) (1997).
13. C. C. Swan and J. S. Arora, 'Topology design of material layout in structured composites of high stiffness and strength', *Struct. Optim.*, **13**, 45–59 (1997).

14. R. Johanson, N. Kikuchi and P. Papalambros, 'Simultaneous topology and material microstructure design, in *Advances in Structural Optimization*, Civil-Comp Press, Edinburgh, 1994, pp. 143–150.
15. Z.-D. Ma, N. Kikuchi, H. -C. Cheng and I. Hagiwara, 'Topology and shape optimization for structural dynamic problems', *ASME-PVP*, **248**, 133–143 (1992).
16. H. C. Gea and Y. Fu, '3-D shell topology optimization using a design domain method', *SAE preprint 951105*, 1995, pp. 245–251.
17. L. H. Tenek and H. Hagiwara, 'Eigenfrequency maximization of plates by optimization of topology using homogenization and mathematical programming', *JSME Int. J., Ser. C: Dyn., Control, Robotics, Des. Manuf.*, **37-4**, 667–677 (1994).
18. C. C. Swan and I. Kosaka, 'Reuss and Voigt mixing rules for variable topology material layout: linear elasticity', *Int. J. Numer. Meth. Engng.*, **40** (1997) submitted for publication.
19. T. Mori and K. Tanaka, 'Average stress in matrix and average elastic energy of materials with misfitting inclusions', *ACTA Metallur.*, **21**, 571–574 (1973).
20. J. Eshelby, 'The determination of the elastic field of an ellipsoidal inclusion and related problems', *Proc. Roy. Soc., London*, **A241**, 379–396 (1957).
21. R. Hill, 'A self-consistent mechanics of composite materials', *J. Mech. Phys. Solids*, **13**, 213–222 (1965).
22. J. M. Guedes, 'Effective properties for non-linear composite materials: computational aspects', in M. P. Bendsoe and C. A. Mota Soares (eds), *Topology Design of Structures*, Kluwer Academic, Publishers, Dordrecht/Boston, 1993, pp. 375–394.
23. P. Pegon and A. Anthoine, 'Numerical strategies for solving continuum damage problems involving softening: application to the homogenization of masonry', in *Advances in Non-Linear Finite Element Methods*, Civil-Comp Press, Edinburgh, 1994.
24. P. M. Suquet, 'Local and global aspects in the mathematical theory of plasticity', in A. Sawczuk and G. Bianchi (eds), *Plasticity today: Modelling Methods and Applications*, Elsevier, London (1985), pp. 279–310.
25. P. M. Suquet, 'Elements of homogenization for inelastic solid mechanics', in E. Sanchez-Palencia and A. Zaoui, (eds), *Homogenization Techniques for Composite Media*, Springer, Berlin, 1987, pp. 193–278.
26. C. C. Swan, 'Techniques for stress and strain controlled homogenization of inelastic periodic composites', *Comput. Meth. Appl. Mech. Engng.*, **117**, 249–267 (1994).
27. J. Aboudi, *Mechanics of Composite Materials: A Unified Micromechanical Approach*, Elsevier, Amsterdam, 1991.
28. A. Bensouan, J.-L. Lions and G. Papanicolaou, 'Asymptotic Analysis for Periodic Structures', North-Holland, Amsterdam, 1978.
29. J. F. Besseling, 'Models of metal plasticity: theory and experiment', in A. Sawczuk and G. Bianchi (eds), *Plasticity Today: Modelling Methods and Applications*, Elsevier, London, 1985, pp. 97–113.
30. C. C. Swan and A. S. Cakmak, 'A hardening orthotropic plasticity model for pressure-insensitive composites: continuum formulation and integration algorithm', *Int. J. Numer. Meth. Engng.*, **37**, 839–860 (1994).
31. W. Voigt, *Wied Ann.*, **38**, (1889).
32. A. Reuss, *Z. Angew. Math. Mech.*, **9**, (1929).
33. J. S. Arora and T. H. Lee, 'Shape design sensitivity analysis of nonlinear nonconservative structural problems', in G. I. N. Rozvany (ed), *Optimization of Large Structural Systems*, Vol. 1, Kluwer Academic Publishers, Dordrecht, (1993), pp. 345–359.
34. M. Ohsaki and J. S. Arora, 'Design sensitivity analysis of elastoplastic structures', *Int. J. Numer. Meth. Engng.*, **37**, 737–762 (1994).
35. C. A. Vidal and R. B. Haber, 'Design sensitivity analysis for rate-independent elastoplasticity', *Comput. Meth. Appl. Mech. Engng.*, **10**, 393–431 (1993).
36. A. Diaz and O. Sigmund, 'Checkerboard patterns in layout optimization', *Struct. Optim.*, **10**, 40–45 (1995).
37. C. S. Jog and R. B. Haber, 'Stability of finite element models for distributed-parameter optimization and topology design', *Comput. Meth. Appl. Mech. Engng.*, **130**, 203–226 (1996).
38. J. C. Simo and R. L. Taylor, 'Consistent tangent operators for rate-independent elastoplasticity', *Comput. Meth. Appl. Mech. Engng.*, **48**, 101–118 (1985).
39. M. Ortiz and J. C. Simo, 'An analysis of a new class of integration algorithms for elasto-plastic constitutive relations', *Int. J. Numer. Meth. Engng.*, **23**, 353–366 (1986).
40. J. C. Simo and R. L. Taylor, 'A return mapping algorithm for plane stress plasticity', *Int. J. Numer. Meth. Engng.*, **22**, 649–670 (1986).
41. M. Ortiz and E. P. Popov, 'Accuracy and stability of integration algorithms for elastoplastic constitutive relations', *Int. J. Numer. Meth. Engng.*, **21**, 1561–1576 (1985).
42. J. Lubliner, *Plasticity Theory*, MacMillan, New York, 1990.
43. J. S. Arora, *IDESIGN Users' Manual Version 4.5.2.*, University of Iowa Technical Report No. ODL-94.08 (1994).
44. T. J. R. Hughes, *The Finite Element Method: Linear Static and Dynamic Finite Element Analysis*, Prentice-Hall, Englewood Cliffs, NJ, 1987.
45. R. R. Mayer, N. Kikuchi and R. A. Scott, 'Application of topological optimization techniques to structural crashworthiness', *Int. J. Numer. Meth. Engng.*, **39**, 1383–1403 (1996).